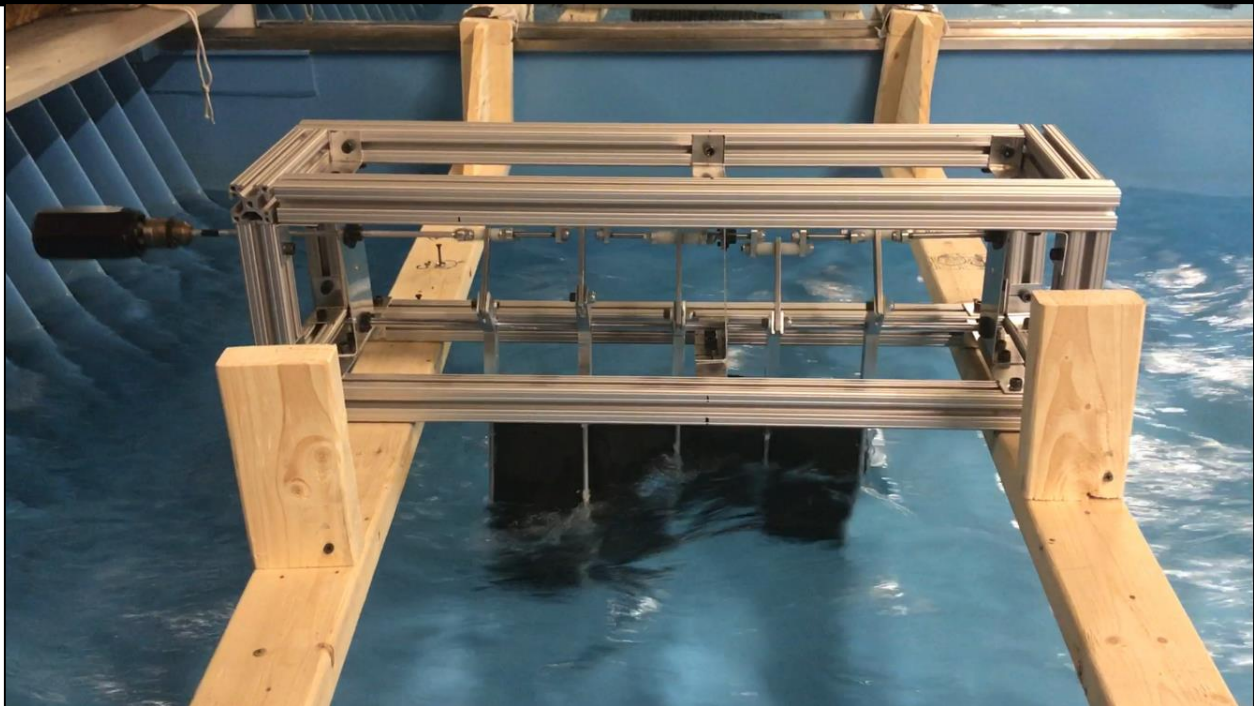2017

Harvesting Hydrokinetic River Current Power

Megan Belval, Hallie Kenyon,
Robert LaFlamme, Sarah Putnam
Worcester Polytechnic Institute

Abstract

An original water energy harvesting mechanism was designed, manufactured, and tested to determine the feasibility of hydropower as a source of renewable energy. The device consists of a neoprene fin that moves in a sinusoidal motion, allowing fish to travel past it. This fin connects to a crankshaft that turns a generator. The device is optimal in low water current speeds, such as rivers or drainage pipes. Five fins of varied thicknesses were tested in water flow speeds between 0.5 m/s and 1.5 m/s using a torque watch and tachometer. The best fin tested was the 1/32" 50A durometer neoprene fin, which produced a power of 1.5 Watts and a 16% efficiency. This efficiency makes the prototype competitive with other water energy harvesting devices on the market and can be theoretically scaled up to have a larger efficiency.

Table of Contents

Table of Figures

Table of Tables

Table of Equations

1.0 Introduction

The world today is facing many problems with sourcing energy for generating power. Fossil fuels are becoming more difficult to harvest, and alternative energy sources are growing. Solar power, wind power, and hydropower are available, yet many of these devices are only feasible for producing power in industrial applications; they are not cost-effective for people who wish to move their homes off consolidated electrical grids and generate their own electricity.

Water has been a source of energy for centuries. Recently, hydropower is harnessed by creating dams for large power plants. These dams, while are considered "clean" sources of energy, can have a major impact on the environment as they displace wildlife and prevent fish from following their migratory patterns. Recently, research and development have focused on creating hydrokinetic power generation devices in the ocean that are not harmful to wildlife. There is a need for more research and development in hydrokinetic power generation, specifically for domestic use that does not pose harmful threats to the environment.

The goal of this project was to produce a working prototype of a device that harvested hydrokinetic river current power. This device is intended to be used in low-current rivers to provide power to single homes as people work to become less dependent upon industrial scale energy production. There are currently no devices commercially available with this purpose.

Initial design decisions were based on recommendations from the 2015 and 2016 Major Qualifying Project (MQP) teams at Worcester Polytechnic Institute (WPI) who started the concept. This year, the team decided to use a crankshaft for power generation. Using a crankshaft over a camshaft reduced friction in the system and eliminated dwell points in the motion of the fin. To develop and improve the design, initial calculations of the force on the fin from water current, and then power output from the crankshaft were calculated. The four-bar linkage of the crankshaft was modeled to find proper dimensions for the device based on the ideal maximum angular deflection. Materials for the fin were investigated and narrowed down to two options: neoprene and silicone. To complete the project, Computer Aided Designs (CAD) of the crankshaft and fin were finalized, the device was manufactured and assembled, and then the prototype was tested to determine a competitive efficiency.

The two main components of the design that the team focused on were the crankshaft and the fin. After the team created computer models, construction began. The crankshaft was manufactured with aluminum. A new frame was created so that the crankshaft could be attached

to the system. For fin construction, the team used four different fin thicknesses and strengths of neoprene. A mold for a silicone fin was also attempted.

The team tested the final design in the WPI Rowing Tank. An apparatus was used to support the device in the tank. A tachometer and torque watch measured the revolutions-per-minute (RPM) and torque of the crankshaft in the water current. This data was used to calculate the power output, efficiency, and tip-speed-ratio of the device during different trials.

2.0 Background

The kinetic energy of moving water such as ocean waves and river currents creates hydropower. Wind, gravity, and differences in water density from temperature and salinity produce water currents. Water energy is the only type of renewable energy that generates 24 hours per day, because river and ocean currents never stop moving. Water has a higher density than wind, so if they were traveling at the same speed, the water would be more powerful. Unfortunately, currents and waves are typically relatively slow and have low frequencies [1]. Engineers are currently focusing on creating hydropower devices to harvest this slow-acting wave force and maximize its power. Water turbines are the most common type of hydropower in use today, but there are many environmental implications with their use. Therefore, the team decided to develop a device that did not use a traditional turbine.

Waves tend to have a general sine pattern, but are often unpredictable and can take many shapes and forms depending on their location [1]. Maintenance is also difficult in the middle of the ocean. For these reasons, this project focused on determining an efficient river current energy device. In order to accomplish this task, the team researched more information regarding different types of river current energy devices that already exist. Although this device will operate in a river, the mechanisms and principles of ocean-powered devices function similarly and may be a baseline for future design work.

2.1 Types of Hydropower

Wave Power Devices
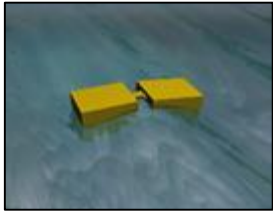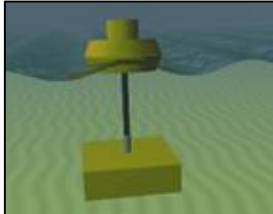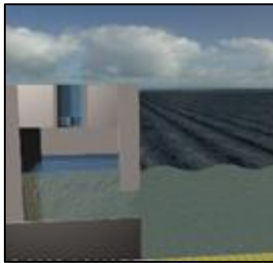
There are two different categories of wave power devices: onshore and offshore. Building a device offshore is more expensive than onshore due to the fees for transporting materials, the complications with installing the power transmission, and the maintenance fees, yet offshore devices can capture greater amounts of energy from stronger currents. Building onshore devices can cause noise pollution for humans, conflict with people living nearby, and interfere with shipping routes depending upon their placement, but they are easier to maintain and more convenient to access [1].

An important consideration for any type of water power device is if it will float at the surface or anchor to the ocean floor. Floating devices have the potential to harvest more kinetic energy since the currents towards the surface are generally stronger and larger [1]. Floor devices

are easier to mount, but have a greater effect on the flora and fauna in the ocean. For this reason, the team decided to create a device that would capture currents towards the surface of a body of water.

There are several floating hydropower devices already engineered. Floating wave power devices are generally categorized by a mechanical component: an attenuator, a point absorber, or an oscillating water column. These components are further explored in Table 1.

Table 1: Primary Power Generation Components [2]

Component	Description	Image
Attenuator	A floating device that operates parallel to the wave direction and rides the wave.	
Point Absorber	Floats and absorbs energy from all directions.	
Oscillating Water Column	Partially submerged and hollow, allowing waves to drive the water column to rise and fall to compress air for the rotation of a turbine.	

If the size of the device is smaller than the periodic length of a wave, then it is called a point absorber. If the size of the device is larger than the periodic length of a wave, then it is called a linear absorber [1]. The energy absorption methods for waves include vertical motion (heave), horizontal motion in the direction the wave is travelling (surge), angular motion about a central axis that is parallel to the crest of the wave (pitch), and angular motion about a vertical axis (yaw) [1]. Additionally, wave profile devices require the force of the waves to react against

another rigid or semi-rigid body. Figure 1 displays the implementation of various wave profile devices in the ocean.
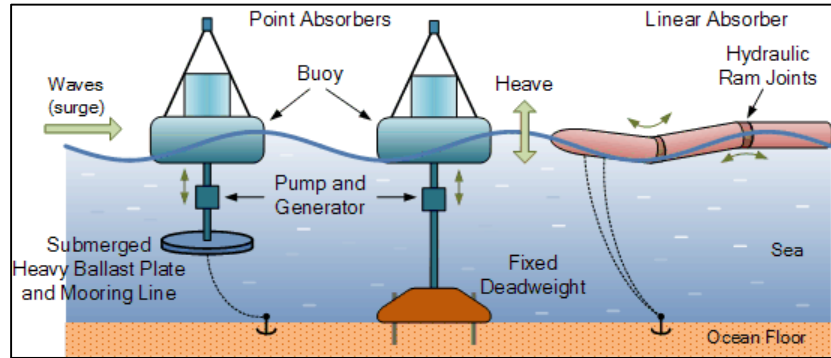
Figure 1: Point and Linear Absorber Generation Systems [1]

Oscillating water columns are normally positioned on or near rocks and cliffs that are next to areas of deep water. The structure of an oscillating water column consists of a natural cave with a blowhole, fabricated chamber, or duct with a wind turbine generator located at the top, above the surface of the water [1]. The constant ebbing and flowing motion of the waves traps water inside the chamber and oscillates in the vertical direction, similar to a piston. In an oscillating water column, a Wells turbine is used because it is able to rotate in the same direction regardless of the direction of the airflow in the column, helping with the conversion efficiency of the system [1]. A few advantages of oscillating water column technology include not producing greenhouse gas emissions and the turbine can be easily removed for repair or maintenance since it is stationed onshore [1]. A disadvantage of oscillating water columns is that the output is dependent on the level of wave energy present. Figure 2 displays the schematic of an oscillating water column system with all of its components.
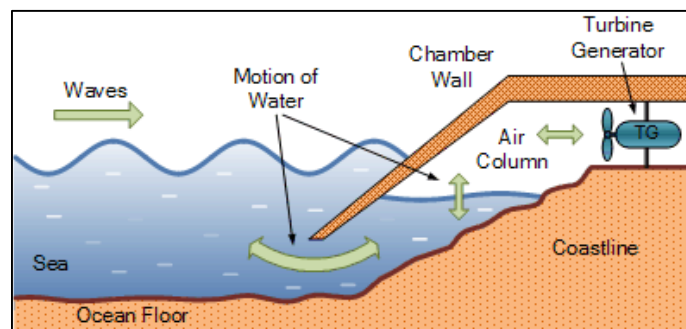
Figure 2: Oscillating Water Column Generation System [1]

Wave capture devices primarily capture the movement of the tides and waves close to the shoreline in order to convert the kinetic energy into potential energy with a holding reservoir. A Kaplan Turbine is typically used to capture and impound the seawater at a height above sea level in order to create a low-head. This reservoir of water can then be drained through the turbine [1]. Figure 3 illustrates a diagram of how the Kaplan Turbine operates.
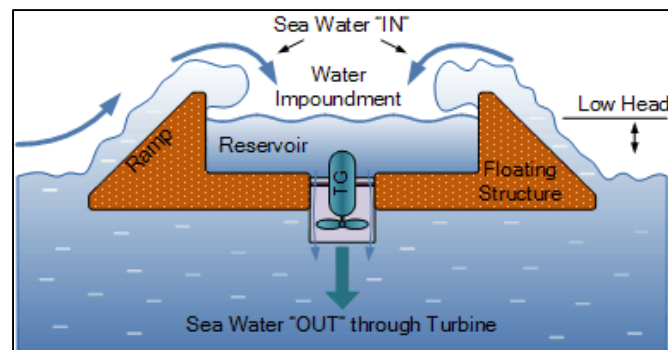
Figure 3: Kaplan Turbine Diagram [1]

River Power Devices

River current energy conversion systems (RCECS) are defined as electromechanical energy converters that employ a river current turbine to harness the kinetic energy of river water [3]. Some of the different types of turbines that are used in RCECS include water current turbines, ultra-low-head hydro turbines, hydrokinetic turbines, free flow or stream turbines, and zero-head hydro turbines [3]. RCECS have been starting to emerge as a feasible solution for harvesting energy. To harness this energy, research needs to be done in order to substantiate the viability of river current energy harvesting devices.

Current Applications and Installations

Many water current harvesting systems exist in the world today. These systems are used to make technological advances in energy harvesting systems for rivers and oceans.

Pelamis Wave Energy Converter

The Pelamis Wave Energy Converter is a wave power device that was created by Pelamis Wave Power in Scotland in 1998. This was the first offshore wave machine to create electricity and send it to the grid. The Pelamis is a series of four tubes, partially submerged in water,

connected by joints that respond to the curvature of the waves. The movement from the water is resisted by hydraulic rams that pump pressurized oil into hydraulic motors. These motors power electric generators to produce electricity. A sealed cable transports the electricity to the shore and can be connected to several devices. The overall power rating for the Pelamis is 750kW and the annual output is 2.7GWh for six to seven meter waves [4]. Figure 4 demonstrates how the motion of the Pelamis is based on the direction of a wave.
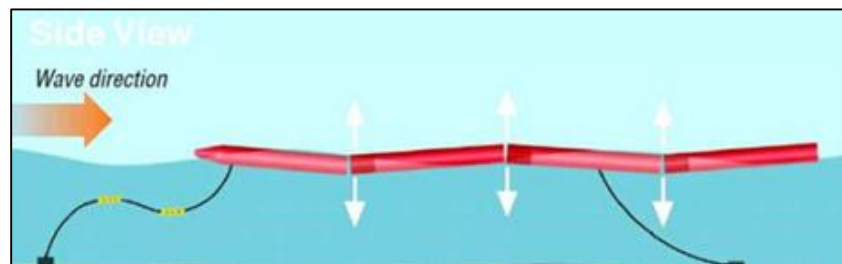
Figure 4: Pelamis Wave Energy Converter [4]

PowerBuoy

PowerBuoy is a wave power device that was created by Ocean Power Technologies in 1997. It consists of a moored system that floats and moves vertically to drive a rack and pinion mechanism, which rotates a generator to produce power. In 2014, Lockheed Martin announced their plan to partner with Ocean Power Technologies' PowerBuoy. They plan to install the world's biggest wave energy project on the coast of Australia with a power capacity to serve the needs of 10,000 homes [2]. The components that allow the PowerBuoy to function are displayed in Figure 5.
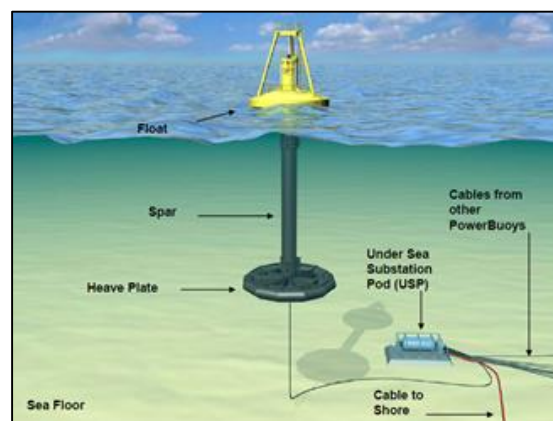
Figure 5: PowerBuoy Energy Harvesting System [2]

CETO

CETO is a wave-energy converter created by Carnegie Wave Industry in Western Australia. As of early 2015, it is the only wave power device in the world that is completely submerged and connected to the grid. The technology is driven by underwater buoys that move up and down with the waves. These buoys push pumps that pressurize seawater delivered to the shore by a pipeline. The onshore high-pressure seawater drives hydroelectric turbines. A desalination plant can use this process to create freshwater with zero emissions [2]. Figure 6 illustrates the components of the CETO and how they work together to create the functioning system.
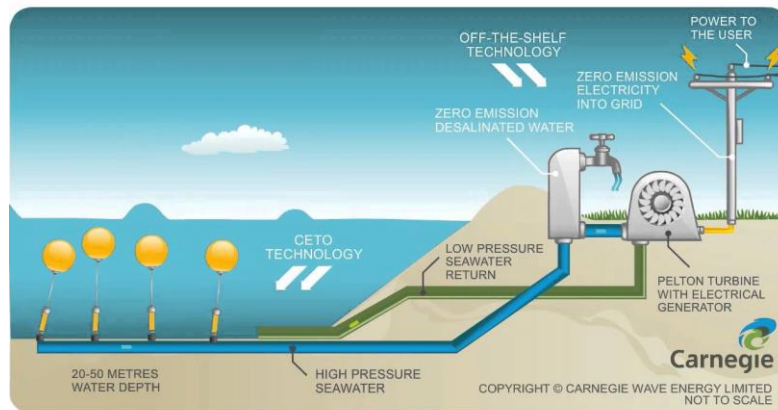
Figure 6: CETO Energy Harvesting System [2]

Smart Turbines

Smart turbines allow energy harvesting from river currents with minimal environmental impact. Traditional turbines for generating hydropower require dams, as they harness the energy from the head of the water. However, these turbines are placed directly in a flowing river current and require no head to harness the kinetic energy the water already has. Each one is able to generate as much as 5kW of power, is easy to install, and requires minimal maintenance. Also, these turbines are designed to not harm fish and other aquatic life as the water flows through them [5]. Additionally, as shown in Figure 7, the turbine has been designed to protect itself from debris floating through the water.
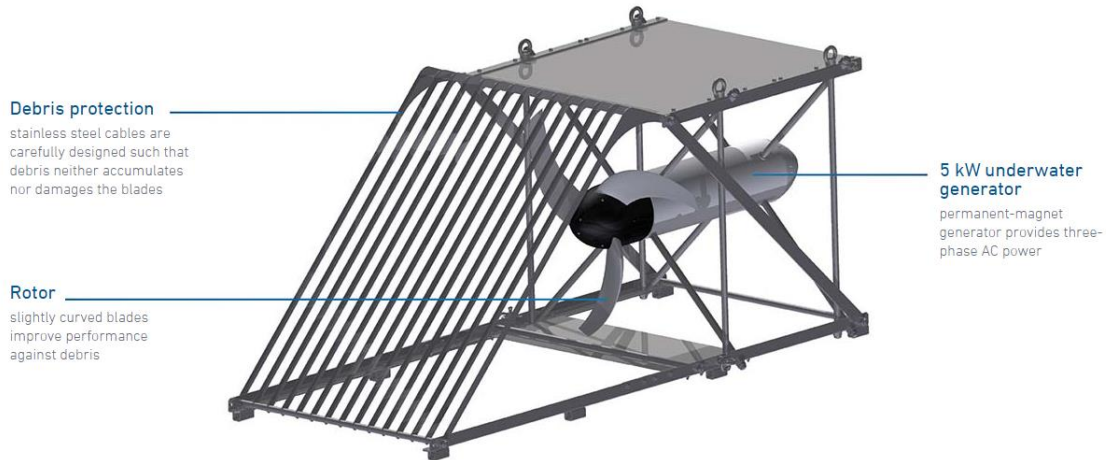
Figure 7: Smart Turbine for No-Head Hydropower Generation [5]

Vortex Induced Vibration for Aquatic Clean Energy (VIVACE)

This device was also designed to capture energy from river currents. It has rigid cylinders mounted to elastic supports which then oscillate as water flows through it. This oscillation creates a changing electrical field. Energy is generated from this flux in the field. VIVACE was designed to gather energy from low flow environments and was tested at the University of Michigan to have an efficiency of 22% at a flow rate of 0.8 m/s [6]. Figure 8 shows the structure of the device.

Figure 8: Vortex Induced Vibration for Aquatic Clean Energy (VIVACE) [7]

2.2 Challenges of Implementing Hydrokinetic Power Generation Devices

There are many challenges associated with implementing hydrokinetic power generation systems. One of the primary challenges is that while many energy sources are capable of predictably producing power, they do not produce a steady, uniform power output in the way that a traditional gas turbine or coal power plant does because they are often subject to changes in weather and changes in season. Figure 9 illustrates the inconsistency of available power from solar, wind, wave, and tidal sources over the course of a year and a day for two separate locations. The top row of the figure is closer to the equator whereas the bottom row is further from the equator.

Daily fluctuations are shown along the horizontal axis and variation over the course of a year is shown along the vertical axis. The color values represent the percentage of energy that is available to be harvested from each source at each time based on the density of each type of energy [8]. Although run-of-river (ROR) systems are not included in Figure 9, river flow rates may vary due to rainfall levels. This leads to non-constant rates of energy generation and potentially longer energy harvesting cycles.
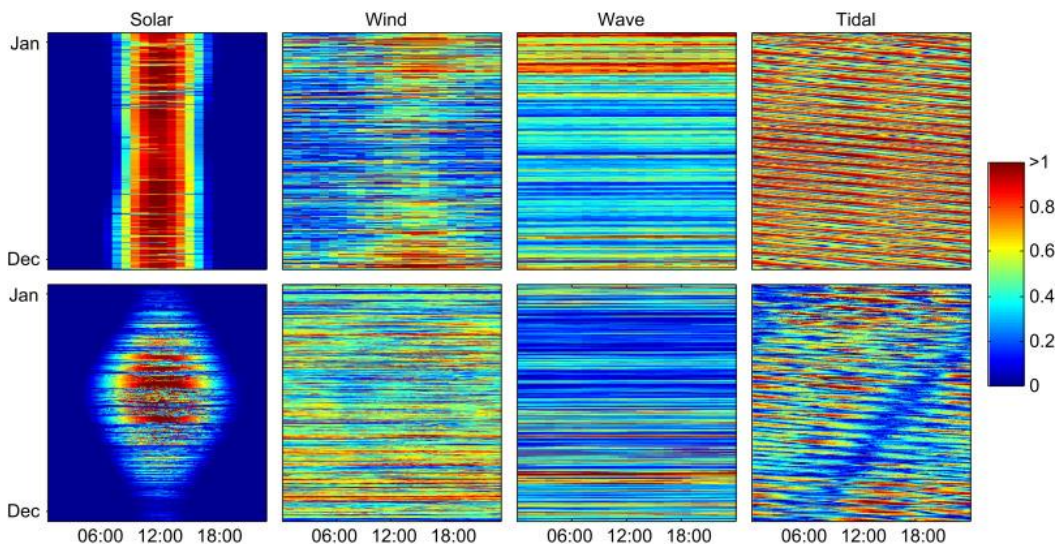
Figure 9: Resource Availability Variability Based upon Time of Year and Time of Day [8]

Maintenance and system durability also pose significant challenges to the design and implementation of ROR systems. There is often sediment and other debris flowing with the water in a river and the water may contain other chemical compounds in it. Debris may cause

damage to the system, sediment may build up, and the other chemicals present may erode the materials within the system. These factors, paired with improper system maintenance, may lead to system failure [9].

An additional challenge associated with ROR hydropower is system placement. Many rivers may be excellent candidates for ROR systems based upon their flow rates and flow volumes, but systems cannot be installed due to environmental protections as well as land and waterway conservation [10].

2.3 Environmental Impact

RORs may alter the way water flows in a given area or change the river's course, leading to changes in the biodiversity within a given area. Changing currents may force fish to change their swimming patterns, may make it more difficult for them to swim in certain places, or may make it impossible for them to migrate through an area. If placed in an area that is also a breeding ground for aquatic wildlife, a ROR system may affect breeding conditions, leading to changes in population numbers [11]. Furthermore, ROR systems pose threats to fish as they may collide while swimming, harming both the fish and the device [12]. These systems not only affect aquatic wildlife but also land animals by disturbing nesting sites, breeding grounds, and feeding areas. Noise from system installation can also negatively impact wildlife [13].

ROR systems also have an effect on the ecological environment. They may cause sedimentation patterns to change as a result of altered currents. This can lead to changes in the plants that are able to grow and can change the profile of biomass that accumulates along the bottom of a river [13]. They can also alter the habitat of endangered and protected species [10]. If multiple systems are installed along one waterway, these effects may be multiplied and have an even greater effect on the surrounding environment [11].

On the other hand, certain aquatic devices can act as artificial ecosystems and help sustain life along the body of water. They can reduce erosion and be used as wave breakers for harbors. Since the wave breakers are already in place, the addition of a hydrokinetic device would not have a drastic effect on the surrounding environment [14].

2.4 Environmental Location

The environment in which any hydrokinetic device is located has an impact on its functionality. Saltwater versus freshwater can help determine the type of materials needed for the device. The flora and fauna ecosystems of both freshwater and saltwater can have an impact on the design and placement of the hydrokinetic device. Additionally, the speed at which the current is flowing is an important parameter to consider when harvesting energy from currents.

The environment can affect how the hydrokinetic device functions. For instance, salt water can corrode certain materials of the device, particularly metal materials [15]. On the other hand, this device could act as an artificial ecosystem, depending on the shape, size, location, and movement [14].

The geographical locations of streams, rivers, lakes, and oceans determine the power and velocity of the water's current. Within the ocean, there are many options for gathering energy from currents. These include rip currents, deep ocean currents, and underwater ocean currents. The different densities in the water are what drives the currents. When the dense cold water sinks to the bottom of the ocean, less dense water moves up to replace it, creating the current [16].

Rip currents in the ocean form when different levels of wave intensity break along the shoreline. They have the potential to produce a lot of power based on the velocities they can reach; however, rip currents do not consistently occur in the exact same spot. This proves challenging when trying to harness its power since the location of rip currents cannot be accurately defined [17]. The currents in rivers vary based on the volume, steepness, gradient, and the topography of the river. When the river's elevation increases or decreases, the potential energy can drastically change [18].

2.5 Biomimicry

For the design of a hydrokinetic device, biomimicry can be beneficial when trying to create an artificial ecosystem while having minimal harm on the surrounding environment. Biomimicry is the use of nature-based ideas, concepts, and movements to find solutions to human challenges [19]. Aquatic biomimicry can be useful when designing the fin for the hydrokinetic device. Mimicking the movement of the flora or fauna that exists in the environment can provide positive results for harnessing energy from the currents.

Some biomimicry designs that have been implemented based on particular aquatic life are the webbed finger and toe designs for flippers and hand paddles. Platypi, for example, have webbing in between their toes and their fingers, thus giving the animal more surface area around their hands and feet, allowing the animal to move more easily in the water. The webbing gives the platypus an opportunity to increase the propulsion force pushing on the resistance of the water. Similarly, competitive and noncompetitive swimmers use flippers and hand paddles to train and to assist in the propulsion of their swimming [20].

Researchers have also mimicked certain fish for their motion in the water. Knife fish and bowfin fish have elongated, ribbon-like, undulating fins, giving these fish a high-performance rate. Figure 10 shows the fin of a knife fish. This particular type of fin allows for precise maneuvering and low-speed stabilization. Additionally, this fin allows for adaptation in calm and slow moving waters [21].

Figure 10: Knife Fish [22]

2.6 Materials

There are multiple considerations to take into account when deciding materials needed in a hydrokinetic device. The material needed to meet certain design criteria that would allow the device to work effectively and efficiently while submerged in the water.

The fin material needed to be durable, manufacturable, and economically feasible. Materials that were considered were neoprene rubber and silicone rubber. The previous MQP projects used neoprene due to its tensile strength, operating temperature range, resistance to water, and appropriate flexibility [23]. The high density of the neoprene made the starting torque for the system higher due to its weight of 985 grams [23]. The previous MQP projects also tested a fin design with a hybrid of neoprene sheets and acrylic plates. The plates helped reduce the folding of the neoprene sheets; however, there were recommendations to fix the design and the

material of the hydrokinetic fin [24]. The team for this project looked into neoprene rubber as a material; however, the thickness and hardness levels varied from previous projects. The durometer is the measure of hardness of the material. Two durometer ratings were researched for the neoprene material: 40A and 50A. To give perspective, a durometer of 40A represents the hardness of a pencil eraser and a durometer of 60A represents the hardness of car tire threading. As the durometer increases, the rubber increases in hardness [25].

Silicone rubber was tested as another option for the fin of the hydrokinetic device and chosen due to its durability and other mechanical properties. When silicone rubber is submerged in water, there is no effect on its electrical properties or its mechanical strength, which allows for a more reliable and durable fin. Additionally, this rubber will only absorb around 1% of water over extended periods. The tear strength of silicone rubber is approximately 9.8 kN/m and the vibration absorption is low, meaning it is not a good vibration insulator [26]. Vibration absorption performance is important when determining the fin material because past groups experienced challenges with the vibrations from the currents and surroundings. Silicone rubber has been used in making equipment for leisure activities such as swimming googles, snorkels, and mouth guards because of its high tear strength, high tensile strength, and physiological inertness [26].

2.7 Previous Projects

2015 Project

The first iteration of this water energy harvesting device was created in 2015 by a group of mechanical engineering students. The device was inspired by the efficiency of an eel's fin, also known as a "ribbon fin." This fin uses rapid propulsion as it oscillates in a sine wave form. The project was designed to focus on low speed flow environments such as rivers and tidal streams. Three prototypes were created, and results showed a production of 14 Watts of power, with a theoretical efficiency of 41% at speeds between 0 and 2 m/s. Constraints considered during the design and development process included stability, ease of manufacture, friction reduction, fin flexibility, and power capture optimization [24].

This project used a crankshaft for its first prototype to convert mechanical reciprocating movement to rotational motion. The ribbon fin spins the output shaft because the pins are not in-line with the main axis of the shaft. An eccentric cam was used in the second prototype, an

eccentric cam was explored. This design was similar to the crankshaft, but the expanded pin encased the shaft so that a single shaft could run through all the mast drivers. The final prototype reduced friction from the bearings by using the cam resting with the follower on a track of 42 steel balls. After testing, it was concluded that the use of a crankshaft would provide greater stability and torsion than the camshaft, and forces from the fin would be eliminated [24].

The number of masts was also varied in this project. Using five masts resulted in a single sine wave at both extremes and at all three points of zero slope along the sine curve. The project team suggested that the number of masts be investigated in the future because a mathematical model suggested a fin with between one and two sine cycles for simplicity of the small-scale prototype. If the wavelength of the fin was too short relative to the number of masts, the fin could fold over. The material of the fin that was the most optimal was a hybrid consisting of acrylic plates and neoprene sewn together for flexibility. Future suggestions for the fin were a fully plated fin with spring joints for increased rigidity and minimal folding [24].

To measure power generated in this project, a fluid pump increased the pressure of the water in order to increase its flow, an inductive motor produced the voltage and the shaft speed, and a friction brake measured shaft speed and monitored torque. A friction brake dynamometer was chosen for its robustness and friction control which eliminated the need for calibration [24].

This device had many potential benefits when compared to other wave power technology, including the following:

- The device has the ability to capture energy from a volume instead of an area of moving fluid [24].
- Small scale iterations of this device can be easily implemented in rivers and larger versions would be placed in oceans [24].
- The optimal power generation was found at low flow speeds, which is unlike most modern hydropower systems that require large gravitational potential for large power generation [24].

There were a few challenges faced in this project:

- The dynamometer skewed the data because its wheel was not perfectly round and the interface with the sensor was not perfectly aligned, increasing friction [24].
- The velocity meter used to collect data lost calibration frequently, especially in a highly turbulent environment, and vibrations altered the data [24].

- When the masts moved into a position where the distances were less than the maximum angular displacement, the excess material on the fin folded [24].
- Excessive force damaged the acrylic in the frame and bent the steel hex shaft [24].
- Torsion in the cams popped the steel balls out and additional support had to be added to the cam-rockers [24].
- Only three heights of fins were tested and could be further investigated [24].
- The WPI pool was used as a testing facility, which consequently resulted in a limited water depth [24].

2016 Project

The second iteration of this water energy harvesting device was created in 2016 by a group of mechanical engineering students. The power efficiency of this device was not found, but the unloaded cut-in speed was measured as 0.7 m/s. Conclusions of this project were that a lighter, continuous fin is necessary for smoother motion and to reduce the torque needed during motion. Future recommendations were to use a different fin material and to improve the manufacturability of the device. Other areas that were explored were fin structure, the drivetrain, the fin-to-crank linkage, and torque-reducing gearing [23].

There were a few changes made to the device by the second project group. In this prototype, the length of the fin was kept at 76.2 cm and the 90-degree transmission angle was kept the same. The number of masts was increased from five to seven, changing the frequency of the fin. The acrylic plating was eliminated to improve the manufacturability of the device. The edges of the neoprene sheets were sewn together to prevent peeling under pressure, and later it was concluded that two sheets were too heavy and prevented the fin from moving [23].

The crankshaft had the same rocker-crank linkage path as the camshaft from the first project group. The crankshaft was spaced so that each journal corresponded to a rocker positioned by the camshaft for interchangeability, and the crankshaft output was a shorter driveshaft mounted at the end of the system [23].

There were a few challenges faced in this project:
- The hybrid camshaft design led to a larger cam assembly and caused dwell points at certain angles of rotation [23].

- The bonding agent was not sticking together as much as it should have been, and the shaft rotated freely [23].
- The correct diameter for the cam was not determined, creating friction points on the shaft and increasing losses [23].

There were several recommendations from this project group for future improvements:
- Using another material like welded aluminum will avoid the potential for slip of the crankshaft. This material may need to be hollow or thin-walled to reduce the weight of the device [23].
- A crankshaft should not be manufactured on campus, but rather a custom crankshaft should be invested in [23].
- A square shaft should be used instead of a hexagonal shaft as the drivetrain and the individual cams should be located at a 90-degree offset from one another [23].
- Based on ANSYS simulation, the fin should incorporate only one sine wave of motion.
- A synthetic fabric should be researched for the fin, such as waterproof canvas, that is thin, light, and water-impermeable [23].
- The shape of the fin should be investigated further because this project group cut slits down parts of the fin for better movement of the masts [23].

A second group worked on the electrical component of this project in 2016. The mechanical output from the fin was low velocity with high torque mechanical power. The conversion to electrical energy required an output reduction to high velocity and low torque mechanical power by a gearbox. The first project group observed a shaft speed of 35 RPM for the hybrid fin. The chosen motor by the electrical group required at least 1000 RPM. Therefore, a motor with a lower RPM range must be chosen for this device, unless the design is scaled up in size [27].

3.0   Design and Construction

The design of this water energy harvesting module took about four weeks to complete, including computations, sketches and computer models. The design was broken into two main categories: the crankshaft and the fin. The fin interacts with the water current and moves in a sinusoidal motion. The fin's motion is translated by the crankshaft and converted to a rotational motion. The rotational motion turns the shaft attached to the generator to create power. All materials used for the construction of this device are listed as follows:

- Stainless steel rods (1/4" diameter)
- Aluminum 80/20
- Aluminum plates (0.0625" thickness)
- Nylon spacers (1/4" shaft diameter)
- ¼ - 20 screws
- ¼ - 20 lock nuts
- Medium-density fiberboard
- Silicone rubber

3.1 Hydroelectric Power Generation

Hydroelectric power does not have losses due to thermodynamic or chemical processes. In this project, kinetic energy from the river current drives the crankshaft, which turns into rotational motion to drive a generator. The initial calculations shown below are used to find the surge force on the fin. The surge force is the force that actually propels the fin through the water. This is an approximation of the possible energy captured by the fin.

Figure 11 shows the geometry of the ribbon fin. By looking at the geometry of this fin, the force from the water on the fin can be calculated. This surge force was used as an estimation of the torque to design the kinematics for the crankshaft.
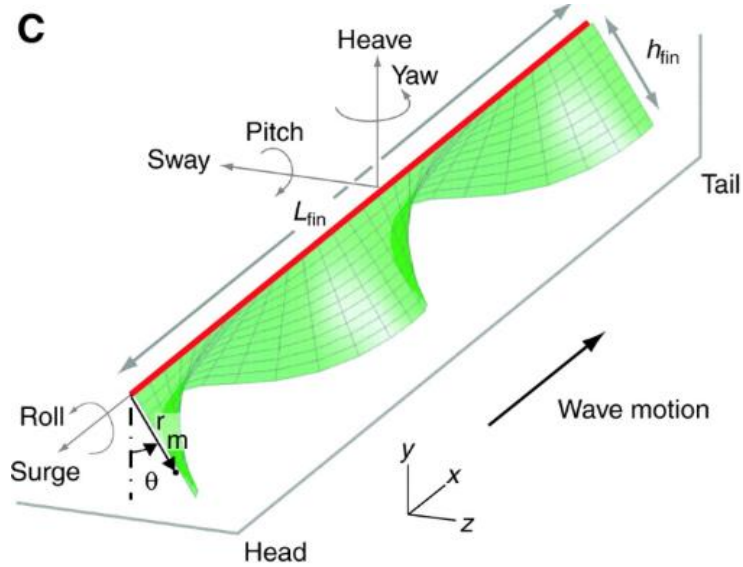
Figure 11: Fin Geometry [23]

$$\lambda = wavelength$$

$$\theta_{max} = max.\ angular\ deflection\ from\ mid\text{-}sagittal\ plane$$

$$f = frequency$$

$$x = coordinate\ in\ axial\ direction$$

$$t = time$$

$$n = number\ of\ 15°\ steps\ between\ masts$$

$$\rho = fluid\ density$$

$$L_{fin} = length\ of\ fin$$

$$h = height\ of\ fin$$

$$C_1 = surge\ force\ constant$$

$$U = velocity\ of\ fin$$

$$\omega = angular\ velocity\ of\ crankshaft$$

$$F_{surge} = surge\ force$$

$$P = power$$

$$\varepsilon = efficiency$$

Equation 1 relates the frequency to the flow speed of the water and the wavelength. The position of the fin based on the time interval of a full oscillation is expressed in Equation 2. This

equation is useful in determining the change in position of the fin over a time interval. The height of the fin used for initial calculations was 0.3048 meters and the length of the fin was 0.762 meters.

$$f = \frac{U}{\lambda}$$

$$f = \frac{2\frac{m}{s}}{.73152m}$$

$$f = 2.734 \; Hz$$

$$\lambda = \frac{360}{15 * 5} * \frac{.762}{5}$$

$$\lambda = .73152m$$

$$\theta(x, t) = \theta_{max} sin2(\frac{x}{\lambda} - ft)$$

$$\theta_{max} = 30°$$

$$\theta_{max} = .5236 \; rad$$

The surge force is dependent upon the angular displacement of the fin (see Equation 3).

$$\emptyset\left(\frac{\lambda}{L_{fin}}\right) = \frac{1 - e^{-\left(\frac{\lambda}{.6L_{fin}}\right)^2}}{\lambda/L_{fin}}$$

$$\emptyset\left(\frac{\lambda}{L_{fin}}\right) = \frac{1 - e^{-\left(\frac{.73152}{.6*.762}\right)^2}}{\frac{.73152}{.762}}$$

$$\emptyset\left(\frac{\lambda}{L_{fin}}\right) = .96114$$

The surge force equation expressed below utilizes the fluid density of water, the surge force constant, the length of the fin, the height of the fin, and the maximum angular deflection of the fin from normal. Equation 4 calculates the force needed to move the fin by evaluating the effect of the fluid density of water moving the fin at maximum angular deflections along its cross-sectional area.

<p style="text-align:center">Equation 4:</p>

$$F_{surge} = C_1 \rho f^2 L_{fin}^4 \theta_{max}^{3.5} \left(\frac{h_{fin}}{L_{fin}} \right) \phi \left(\frac{\lambda}{L_{fin}} \right)$$

$$F_{surge} = (86.03) \left(\frac{1000 kg}{m^3} \right) (2.734 Hz)^2 (.762)^4 (.5236)^{3.5} \left(\frac{.3048m}{.762m} \right)^{3.9} * .96114$$

$$F_{surge} = 607.28 \ N$$

An estimate of the torque and power output of the crankshaft due to the surge force can be found by in Equations 5-8. The calculated surge force was 607.28 N and this value was used to calculate the torque of the system. The angular velocity was determined by taking the derivative of the vertical component of the fin's angular displacement. The power input was then used to calculate the power output of the fin.

<p style="text-align:center">Equation 5:</p>

$$T_{in} = F sin\theta h$$

$$T_{in} = 607.28 sin\theta h$$
$$T_{in} = 607.28 \sin(30)(.3048)$$
$$T_{in} = 92.5 Nm$$

<p style="text-align:center">When $\theta = \theta_{max}$ at time t=2s:</p>
<p style="text-align:center">Equation 6:</p>

$$\omega_{in} = cos\theta t$$

$$\omega_{in} = \cos(30)(2)$$

$$\omega_{in} = 1.73 \text{ rad/s}$$

Equation 7:

$$P_{in} = T_{in} * \omega_{in}$$

$$P_{in} = 92.5N * 1.73 \, rad/s$$
$$P_{in} = 160.2W$$

Equation 8:

$$P_{in}\left(\varepsilon_{system}\right) = P_{out}$$

$$.50 < \varepsilon_{system} < .75$$
$$(160.2W)(.50) < P_{out} < (160.2W)(.75)$$
$$P_{out} = 80.1W \text{ to } 120.15W$$

3.2 Frame

The water energy harvesting module is contained in a frame composed of aluminum 80/20 bar stock. The frame is made from pieces of lengths: 6.5", 8", and 30" cut by a band saw. Because the 80/20 is 1.5" thick, the frame, when put together, is 30" long, 8" wide, and 8" tall. Each piece was sanded for smooth edges before bolted together.

To connect the pieces of the frame, a custom bracket was designed from sheet metal of thickness 0.0625". The brackets were cut out as 1" by 3" rectangles using a shear. Two holes were drilled in each bracket with a 3/8" drill bit 0.075" from either side of the center of the piece as seen below. These brackets were then bent along the centerline to a ninety-degree angle and sanded. These brackets were used at each point of contact in the corners between 80/20 pieces and fastened together using 1/4-20 bolts and nuts. Figure 12 shows the SolidWorks model of the frame.
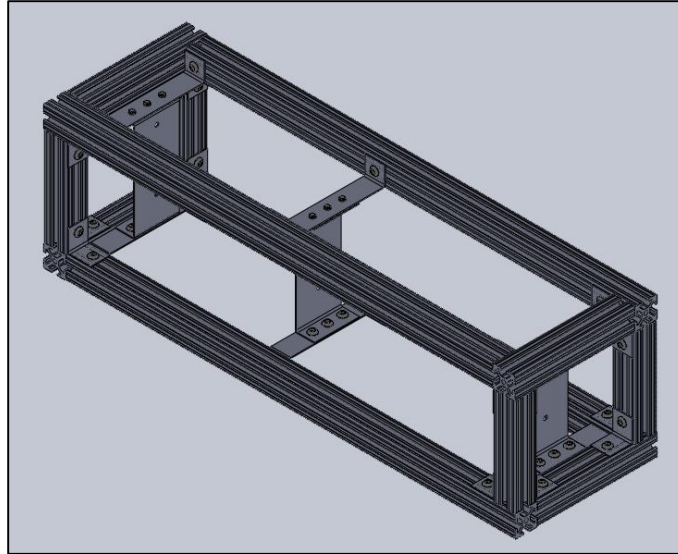
Figure 12: SolidWorks Representation of the Frame Used to House the Crankshaft and Fin Mechanisms

3.3 Crankshaft Design

A crankshaft was designed to harness the power created by the fin. A crankshaft can either turn generating energy into power or can dissipate the power output of a motor. In this application, it was used to generate power. The crankshaft consisted of a main shaft with offset sections that rotate the main shaft when pushed by an attached linkage. The linkage was built to ensure that the crankshaft could fully rotate and also restrict the cross-sectional motion of the fin to +/- 15º from normal. This shaft could be easily connected to a generator.

Traditionally, crankshafts are used in automotive applications. They run along the length of an engine, and as the pistons fire, they push rods that are connected to offset sections of the shaft, causing it to turn. This connects to the transmission and eventually drives the wheels of the automotive [28]. Figure 13 shows a typical automotive crankshaft.

Figure 13: Typical Automotive Crankshaft [28]

A crankshaft was chosen for this application because the shaft and associated linkage system could be easily scaled to prototype and did not take up much vertical space above the fin. Friction could be minimized throughout the linkage through the use of ball bearings. Additionally, the spacing around the shaft of the offset sections, also called journals, could be easily controlled. The motion of the fin was designed to follow a generic sine curve. Masts that connect the fin to the crankshaft linkage were placed every ninety-degrees along the curve, and the journals of the shaft were offset from each other by ninety degrees.

The linkage to connect the crankshaft was designed to restrict the path of motion of the fin to a thirty-degree range, as suggested by previous project groups, and to fit within the frame. It was also designed to minimize the offset of the journals from the crankshaft in order to maximize the rotational output of the shaft. The crankshaft parameters are displayed in the analysis below. Figure 14 shows the corresponding outline for the design.
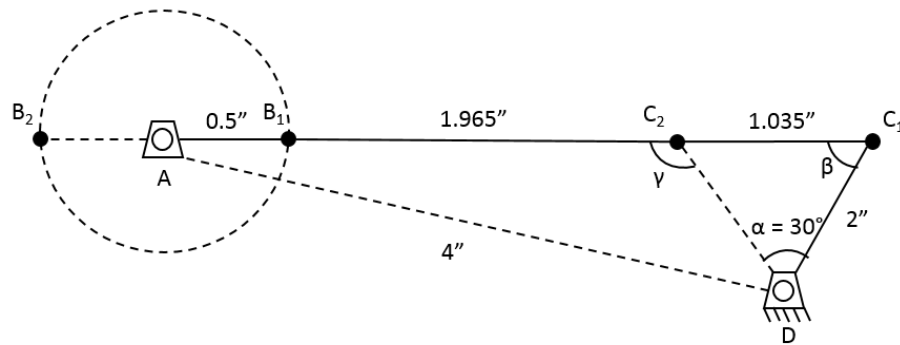
Figure 14: Sketch of Design for an Individual Crank on the Crankshaft

Crankshaft Design Analysis:

Given:

$$AB_1 = 0.5"$$

$$AB_2 = 0.5"$$

$$C_1D = 2"$$

$$C_2D = 2"$$

$$AD = 4"$$

$$\alpha = 30°$$

To determine the angles:

$$\beta = \frac{180° - \alpha}{2}$$

$$\gamma = 180° - \alpha$$

$$\beta = 75°$$

$$\gamma = 105°$$

Law of sines:

$$\frac{sin75°}{2} = \frac{sin30°}{C_1C_2}$$

$$C_1C_2 = 1.035"$$

Law of cosines:

$$c^2 = a^2 + b^2 + 2ab * cosC$$

$$4^2 = 2^2 + (1+x)^2 - 2*2*(1+x)*cos105°$$

$$12 = 1 + 2x + x^2 + 1.035 + 1.035x$$

$$x^2 + 3.0353x - 9.9647 = 0$$

$$x = 1.9849"$$

$$BC = x + C_1C_2$$

$$BC = 1.9849 + 1.035 = 3.0202" \approx 3"$$

Additionally, an atlas of linkages was used to ensure that the path of the designed linkage would match the path needed for the fin. As shown in Figure 15, the center of the path is offset from the vertical axis. Therefore, the piece connecting the fin to the linkage needed to be angled to properly transfer the motion of the fin to the linkage.

Figure 15: Point "C" Shows the Path of the Fin, as Constrained by the Crankshaft

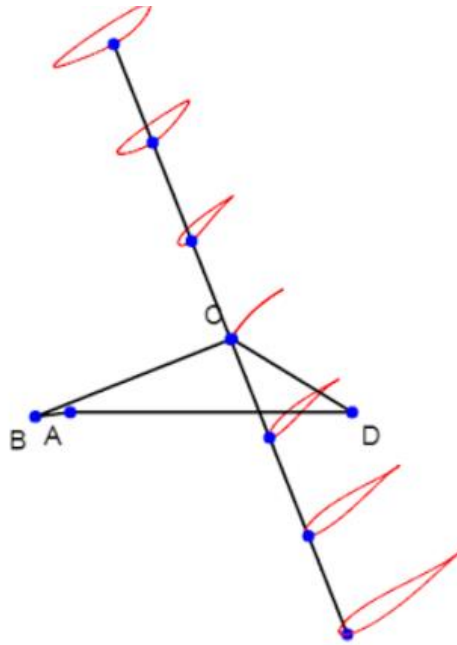Equation 9 shows the calculation of angular offset and Figure 16 displays the configuration of the variables with reference to the linkage.
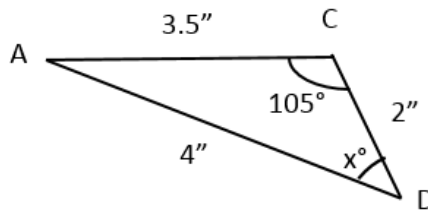

Figure 16: Angle ADC Is the Angular Offset That Occurs as a Result of the Crankshaft

Equation 9:

$$\frac{\sin 105°}{4} = \frac{\sin x}{3.5}$$

$$x = 57.69°$$

3.4 Crankshaft Construction

Traditionally, the pieces of a crankshaft are welded together, as this gives it strength and rigidity and ensures that the journals are properly offset from each other. Due to temporal, monetary, and skill constraints, the crankshaft was built out of pieces that threaded together and locked into place using standard lock nuts. The crankshaft and linkage system was composed of the following parts: threaded rods, threaded cranks, an intermediary linkage piece, and a piece to transfer the motion from the fin to the linkage. The threaded crank corresponds to Link AB, the intermediary linkage piece corresponds to Link BC, the piece to transfer the motion from the fin to the crank corresponds to Link CD, and Link AD corresponds to the distance between the center of the crankshaft (point A) and the shaft supporting all of the links connecting to the fin (point D). Figure 17 shows the constructed crankshaft.

Figure 17: Assembled Crankshaft Outside of the Frame

Quarter inch diameter chrome plated carbon steel shaft was used to create the threaded rods. The shaft was cut into seven three-inch sections and two five-inch sections. This was the length needed to properly space the journals of the crankshaft and the masts of the fin within the frame. The SolidWorks design for the part is shown in Figure 18. A single point threading tool in a computer numerical control (CNC) lathe was used to create ¼-20 threading on both ends of the three-inch sections and one end of the five-inch sections. Esprit was used to create the G-code for the lathe. A belt sander was used to finish the piece and smooth all rough edges.
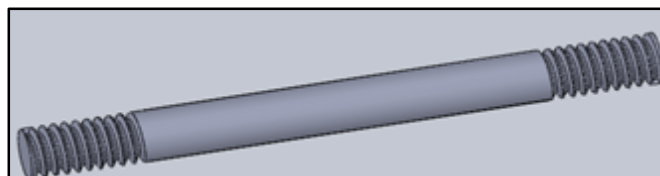
Figure 18: SolidWorks Model of the Threaded Rod Used in the Crankshaft

The second component of the crankshaft system is Link AB. Eleven of these links were needed to build the crankshaft. SolidWorks was used to design the piece and a series of Esprit files were made to manufacture it using a CNC mill. The parts were all cut from the same piece of stock. The first program drilled and threaded all of the holes for the parts using a number 7 drill bit. They were then threaded using a ¼-20 tap. Lastly, the pieces were cut out from the sheet. The pieces are sized so that the centers of the holes are a half-inch apart. The final part is shown in Figure 19.

Figure 19: Link AB

The designs for Link BC, five of which were needed for the prototype, were also created in SolidWorks and an Esprit program was developed to create the two five-eighths inch holes, spaced three inches apart. These holes were then made using a CNC mill. After the holes were made the pieces were cut to size. Ball bearings were then press fitted into five-eighths inch holes in order to reduce the friction between the links as the system moved. The finished piece is shown in Figure 20.

Figure 20: Finished Link BC Component

Lastly, Link CD was created from a SolidWorks model and a series of Esprit programs and was fabricated in a CNC mill. The five parts were all cut from the same piece of stock. The first Esprit program drilled all holes for the part, each a quarter-inch across. It also created the five-eighths inch diameter counter bore into which a ball bearing would later be press fit. Two of the holes created were quarter-inch construction holes. This sheet was then bolted to a construction block. The second Esprit program cut all the pieces out from the block and the construction block held the pieces in place while the mill cut them out. The third and final

program was used to cut a slot in the base of the link to allow it to connect to Link BC. Upon completion of these steps, a ¼-20 threaded hole was tapped and threaded in the top of the link to allow the masts of the fin to screw into it. Finally, a ball bearing was press fit into the center hole of the link. The finished piece is shown in Figures 21 and 22.

Figure 21: Side View of Link CD

Figure 22: Top View of Link CD to Highlight the Slot at the Bottom of the Piece

3.5 Crankshaft Assembly

After all the pieces were fabricated, the crankshaft was put together within the frame for the fin. Each Link BC was placed in the middle of a threaded rod and held in place with nylon spacers. These rods acted as the journals of the crankshaft. They were connected to one of the Link AB pieces on either end and locked in place using a lock nut as shown in Figure 23. After these five pieces of the crankshaft were put together, the rest of the threaded rods connected these pieces and locked the journals into the proper orientation, each ninety degrees apart. The

crankshaft was also attached to the fin frame and held in place with shoulder screws. Sheet metal ball bearings were used to ensure the shaft could rotate freely within the frame. Each Link BC piece was then connected to a Link CD piece using a shoulder screw and lock nuts. The top of Link BC fit into the slot of Link CD and rotated freely. Finally, a support shaft was placed through the center hole of the ball bearings in each Link CD to hold them in place. The support shaft was also held in place with shoulder screws. To further stabilize the linkages, plastic tubing was placed around each Link CD on the support shaft.

Figure 23: Link BC Connected to Link AB

3.6 Fin Masts

Five masts were equally spaced along the fin to simulate a complete sine wave. Each mast was made from aluminum and was ¼" in diameter. The two outer masts were 11" in length, the mast in the middle was 12.4" long, and the other two masts were 12" long. These five masts screwed into the Links BC so that the motion created by the crankshaft translated into the sinusoidal motion of the fin masts, and ultimately the fin itself.

Each mast was cut to length using a vertical band saw and was then sanded. From there, ½" of one end of each mast was given a ¼-20 thread so that the height of each mast, when fully screwed in, would fit the dimensions of the designed fins.

3.7 Fin

After researching information on different materials within CES Edupack, a material property database, and reviewing the information gathered on materials from previous groups, neoprene rubber was chosen due to its durability and flexibility. A series of four neoprene fins of varying thickness and durometers were fabricated for testing. They were as follows: 1/32" with a

durometer of 40A, 1/32" with a durometer of 50A, 3/32" with a durometer of 50A, and 1/8" with a durometer of 50A.

Neoprene sheets of the desired thicknesses were purchased and cut to length and shape using a box-cutter. Each sheet was cut to a length of 36" and to a height of 12". Then, each sheet was cut at the top into the arch shape. The shape of the arch matched the height of each fin mast based on the angular displacement of the masts when the system was assembled.

Finally, holes were poked through each sheet approximately 1.5" apart along the height of the fin using an awl. This ensured that the fins could be easily attached around the masts and be quickly interchanged during testing. They were attached to the masts using zip ties.
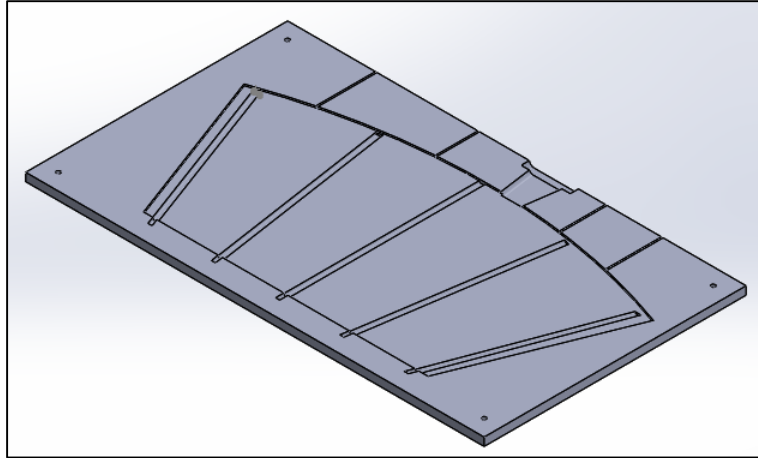
3.8 Fin Mold

To create an additional fin, the team attempted to cast a silicone fin from a mold. The purpose of the mold was to create a better system for attaching the fin to the rods and to reduce friction between the fin and the water. Pockets were made in the fin for the rods to slide into. The goal of the pockets was to keep the rods secure while the fin and crankshaft moved with the water currents.

The mold was made from medium density fiberboard and sealed with Krylon Crystal Clear. Silicone was chosen for its durability as well as its simplicity in the casting process. One challenge with silicone was that the material easily develops porosity[1]. To mitigate this issue during casting, the mold was tapped and shaken to release air bubbles.

The mold was initially designed in SolidWorks, as seen Figure 24. The length of the cast fin was 24", the maximum height was 12" and the overall thickness of the casting was 3/32". The rods were spaced 4" apart along the bottom and 5" apart along the top, which created the shape of a fan. The length of the rods varied, and therefore the length of the pockets inside the fin mold also varied. The outer rod pockets were 10.5" long, the inner rod pockets were 11.5" long, and the middle rod was 12" long. The goal of the varying rod lengths was to increase stability and movement of the fin.

---

[1] Porosity is the presence of air bubbles in a material after it has been cast. It can lead to surface defects and lower strength and ductility properties within a material.

Figure 24: Fin Mold

When constructing the fin mold, the medium density fiberboard (MDF) was cut using a CNC mill. Two similar molds were made, as the molds were symmetrical. Smooth-On Universal Mold Release was put on the surface of the mold and the masts to help the casting to come out easily. The two molds were bolted together with the masts located in the pockets. This ensured that there would be exactly enough space for the rods to fit when they were attached to the crankshaft and structure. The silicone rubber came as a two-part compound that had to be mixed together. Once it was ready, it was poured into the mold and left to cure for twenty-four hours.

The casting of the fin was not successful. Once the silicone had set and the mold was taken apart, the casting was not consistent and had not filled the mold cavity. Although sealant and mold release were used to cover the surface of the mold, moisture from the silicone was absorbed into the MDF and the volume of silicone was reduced. Another reason the mold was not successful was because the surface of the MDF was not smooth due to the size of the particles used to make the board. Even though the surface of the mold had been smoothed, the surface of the material that was molded was rough, so even if there had been enough material, it would have been too rough to work well in the water, especially compared to the smoothness of the neoprene. Overall, the idea to cast a fin out of silicone rubber was a good experiment, but due to temporal and budgetary constraints, it was not successful.

4.0 Testing Results and Analysis

4.1 Testing Procedure

The device was tested in the rowing tank facility at WPI. This facility is capable of water flow speeds up to 2 m/s. For set up, the device was secured between two wooden planks, which were designed to support the size and weight of the hydrokinetic device and fit within the rowing tank dimensions. Unfortunately, the height of the water in the tank could not be altered, so only half of the fin was submerged in the water. Four neoprene fins of different thicknesses were tested: 1/32" 50A durometer, 3/32" 50A durometer, 1/32" 40A durometer, and 1/8" 50A durometer. Each fin was tested three times at 0.5 m/s, 0.75 m/s, 1 m/s, and 1.25 m/s current speeds. These results were averaged in plots to find the best conditions for the tested fins.

The goal of testing fins of different thicknesses was to compare their maximum rotational speed and torque from different water currents in order to determine power output. This power output was an overestimate, but it was used as a maximum to interpolate the rest of the data. RPM and torque were measured using a tachometer and a torque watch, respectively. The tachometer, shown in Figure 25, was held above the rotating crankshaft, which had an adhesive reflector attached it. It had a rating accuracy of +/- 0.05% and could take readings between two and twenty inches from the rotating shaft. As the shaft rotated, the laser from the tachometer reflected infrared light off the reflector back to the measuring device. This digitally gathered the rotational speed based on the number of times the reflector passed the tachometer in one minute. The maximum RPM of the crankshaft was measured when there was no load on the shaft for each trial, and was then recorded.
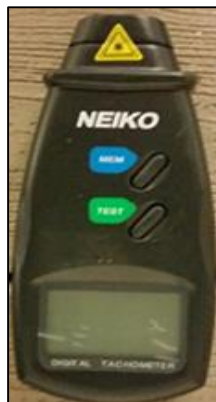

Figure 25: Tachometer

The maximum torque exerted by the device had a large range; therefore, two different torque watches were used to measure it, as shown in Figure 26. The first torque watch accurately read torques between 2 and 40 in-oz. and the second accurately read torques between 15 and 100 in-oz. Both instruments had an accuracy of +/- 2%.

Figure 26: Torque Watch (50 in-oz., 100 in-oz.)

Each torque watch was attached directly to the rotating crankshaft, as seen in Figure 27, to measure the maximum output torque due to the normal forces from the water on the fin. This maximum torque was achieved and recorded when the shaft was held at a complete stop while water was still flowing and the RPM was zero.
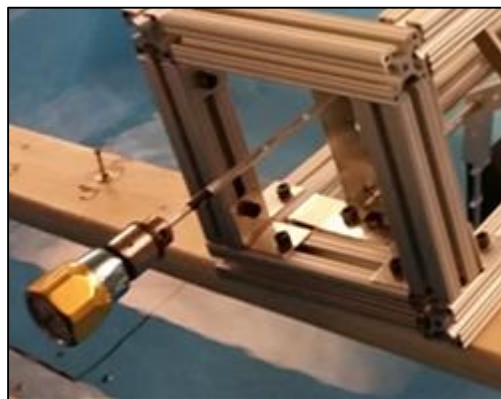
Figure 27: Torque Watch on the Crankshaft

4.2 Results and Analysis

The actual maximum power output and the theoretical maximum power output were calculated and used to determine the maximum efficiency of each fin. The actual power output

was calculated with the following equation. This equation multiplied the torque and angular velocity data recorded from the crankshaft in each trial. An example calculation of the best performing fin is displayed in Equation 10.

Equation 10:

$$P = \tau\omega$$

$$\tau = Torque$$
$$\omega = angular\ velocity$$

Example Calculation for 1/32" 50A Fin at 1.0 m/s:

Torque in in-oz.:

$$\tau = 74.0\ in - oz.$$

Conversion from in-oz. to Nm:

$$1\ in - oz. =\ 0.00706\ Nm$$

Torque in Nm:

$$\tau = 0.5224\ Nm$$

Angular velocity of the crankshaft at this speed:

$$\omega = 112.6\ rotations/minute$$

Angular velocity in SI units:

$$\omega = 1.877\ rotations/second$$

Actual maximum power output for this fin trial:

$$P = \tau\omega$$
$$P = (0.5224\ Nm) * (1.877\ rotations/second)$$
$$P = 0.98\ W$$

The theoretical power output of each fin was determined using the dynamic pressure equation multiplied by the volumetric flow rate. Equation 11 displays dynamic pressure using the density of water and the velocity of the water. The volumetric flow rate was calculated from the velocity of the water and the cross-sectional area of each fin normal to the current, expressed in Equation 12. This cross-sectional area was calculated from the amplitude of the sine wave and the height of the fin.

Equation 11:

$$P_{out} = \frac{1}{2}\rho v^2 Q$$

Equation 12:

$$Q = VA$$

$$\rho = density$$
$$Q = volumetric\ flow\ rate$$
$$V = flow\ velocity$$
$$A = cross\ section\ area\ of\ fin\ normal\ to\ current$$

Example Calculation for 1/32" 50A Fin at 1.0 m/s:

Cross-sectional area of the fin (shown in Figure 11):
$$A = \sin(15°) * 12in * 6in$$
$$A = 18.63\ in^2$$
$$A = 0.012\ m^2$$

Theoretical maximum power:

Equation 13:

$$P_{out} = \frac{1}{2}\rho v^2 Q$$

$$P_{out} = \frac{1}{2}\rho v^3 A$$

$$P_{out} = \frac{1}{2}\left(1000\frac{kg}{m^3}\right)\left(1.0\frac{m}{s}\right)^3 (0.012\ m^2)$$

$$P_{out} = 6.0\ W$$

The actual power was divided by the theoretical power to calculate the efficiency of each fin, as seen in the equation and example below.

Equation 14:

$$\%\ efficiency = \frac{P}{P_{out}} * 100\%$$

Example Calculation for 1/32" 50A Fin at 1.0 m/s:

$$\%\ efficiency = \frac{1.0}{6.0} * 100\%$$

$$\%\ efficiency = 16\%$$

This data and these calculations were put into tables and then graphed for analysis. The first graph for each fin displays its efficiency curve for the fin. It plots the efficiency of the fin against the speed of the water current and shows the speed at which the fin functions most efficiently. As the current increases, the energy available within the water steadily increases and the energy harvested by the fin increases. However, they do not increase at the same rate. Initially the efficiency increases as the current speed increases until it reaches a maximum point, after which the efficiency of the device will decrease, even though the power output is increasing. Because of this relationship, the ideal curve for this graph is parabolic.

The second graph plots the efficiency of the fin against the torque of the crankshaft to show the effect of increasing the torque on the efficiency of the device. Ideally, this graph has a shape similar to the efficiency curve, as torque and current speed are directly related.

The third graph plots the relationship between the torque and the RPM of the crankshaft. Torque and RPM are both directly related to the current speed of the water, and should ideally have a linear relationship when graphed.

The fourth graph shows the relationship between the power generated by the fin and the torque generated by the crankshaft. Torque is a necessary component of the power equation and this graph shows the effect that changing torque has on the power that can be produced by the device. This relationship should be a polynomial function with a positive slope.

The fifth graph shows the relationship between the efficiency of the fin and the ratio of the tip speed of the fin and the speed of the current. The tip speed of the fin is the velocity of the edge of the fin normal to the water current. This graph is similar to the efficiency graph because there is a maximum power output when the speed of the edge of the fin is closest to the actual speed of the water flow.

1/32" 50A Durometer

The first fin tested was constructed out of 1/32" 50A durometer neoprene. Two fins tested were this thick, but this fin had a higher durometer than the other fin. Table 2 shows the speed of the water current, the maximum torque of the crankshaft, the RPM of the crankshaft with no load, the actual power, theoretical power, efficiency, and tip speed ratio for each trial. This fin did not move at any water current speeds below 0.50 m/s because there was not enough force on the fin to overcome the static frictional force of the fin, or the threshold for motion. The fin produced no data at any speed above 1.25 m/s because the force from the water current was too large and caused the neoprene to fold over and "bunch up" on the masts, preventing the fin from oscillating in the water.

Thickness: 1/32" 50A						
Speed (m/s)	Torque (in-oz)	RPM	Power (W)	P	Efficiency	ωR/u
0.25	0	0	0.0	0.0	0%	0.0
0.50	12	33	0.0	0.8	6%	0.5
0.50	17	30	0.1	0.8	8%	0.5
0.50	19	36	0.1	0.8	11%	0.6
0.75	50	64	0.4	2.5	15%	0.7
0.75	55	63	0.4	2.5	16%	0.7
0.75	50	68	0.4	2.5	16%	0.8
1.00	64	104	0.8	6.0	13%	0.9
1.00	72	110	0.9	6.0	15%	0.9
1.00	74	113	1.0	6.0	16%	0.9
1.25	95	127	1.4	11.7	12%	0.8
1.25	96	128	1.4	11.7	12%	0.8
1.25	94	134	1.5	11.7	13%	0.9
1.50	0	0	0.0	0.0	0%	0.0

The 1/32" 50A durometer fin reached a torque between 12 in-oz. and 96 in-oz., and an RPM between 30 and 134. These measured values produced power ratings between 0.1 Watts and 1.5 Watts, with a maximum efficiency of 16%.

The maximum efficiency measured was 16% at 112 RPM with a 74 in-oz. torque. This was the maximum overall efficiency measured for any fin tested. As shown in Figure 24, efficiency and current speed have a parabolic relationship; after the peak, the efficiency decreased while the current speed continued to increase. The RPM and torque of the crankshaft had a direct relationship with the flow speed of the water. However, the torque did not increase in a consistent interval with higher flow speeds. This is why the efficiency of the fin decreased at the end of the curve. Based on the parabolic curve in Figure 28, the best water flow speed for the 1/32" 50A durometer fin is approximately 0.95 m/s.
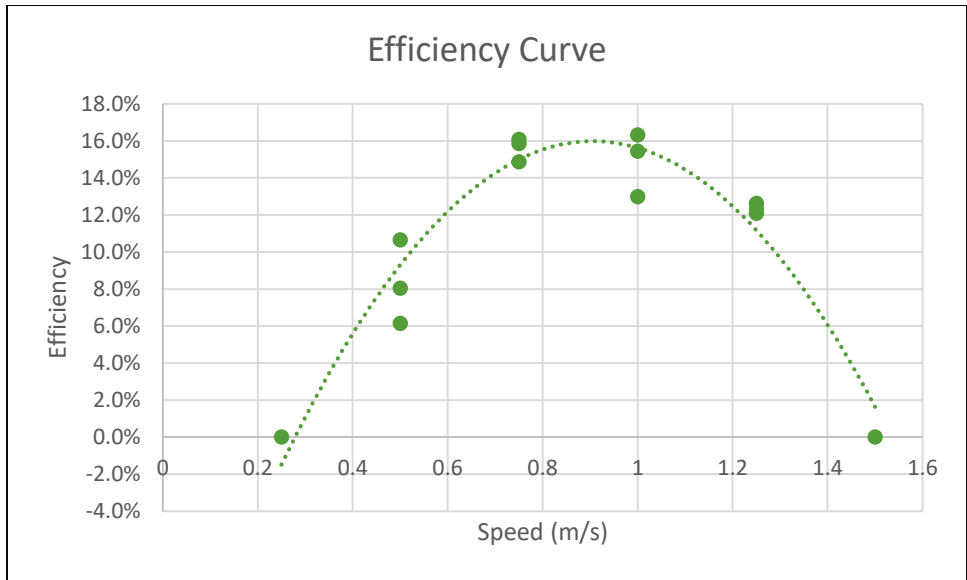
Figure 28: 1/32" 50A Efficiency Curve

The curve in Figure 29 shows that the maximum efficiency for this fin occurred when the torque was 60 in-oz. The efficiency and torque have a parabolic relationship, similar to the efficiency vs. speed graph. After the peak, the torque slowly increased while the efficiency decreased.
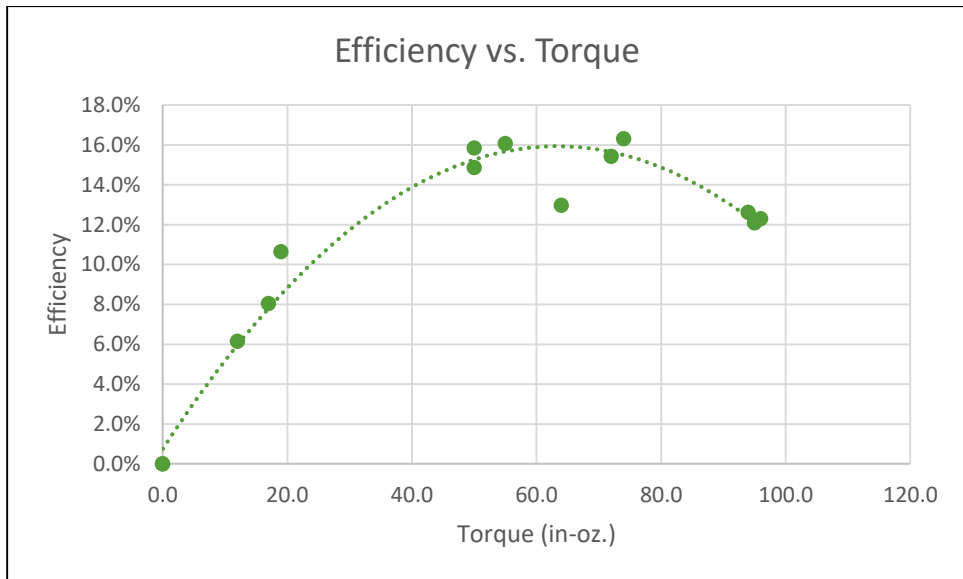

Figure 29: 1/32" 50A Efficiency vs. Torque Graph

Figure 30 shows that torque and RPM have a direct relationship; as the RPM increased, the torque also increased. As mentioned in the testing procedure, the data collected only goes up to 100 in-oz. since the torque watch did not measure beyond this torque value. At the maximum torque reading of 96 in-oz., the device reached a reading of 128 RPM, as displayed in Figure 30.
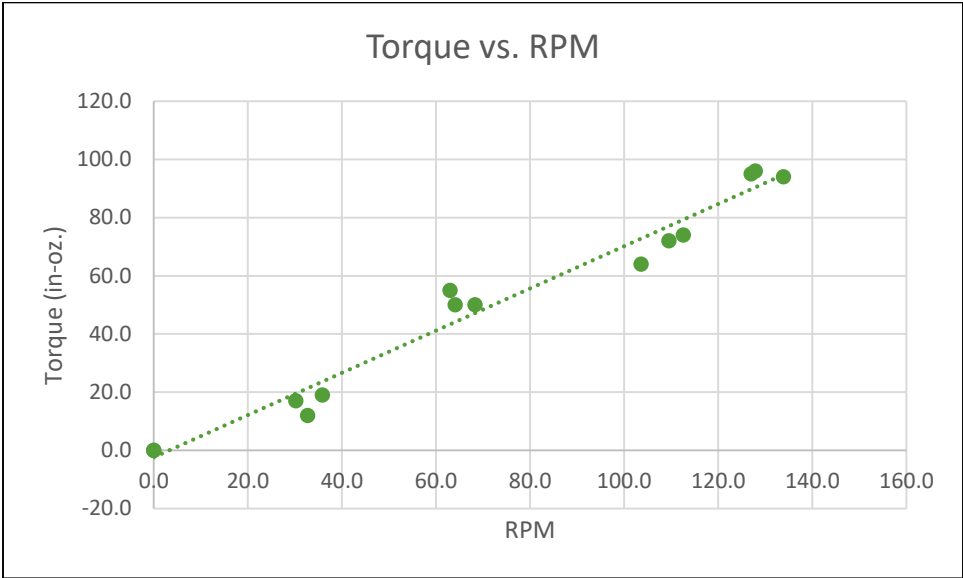

Figure 30: 1/32" 50A Torque vs. RPM Graph

The theoretical maximum power output was calculated based on the gathered data. Figure 31 shows the relationship between the calculated power and the torque measured. There was no maximum power found from this data due to the limitations of the fin and the crankshaft. These limitations included the size of the surface area of the fin normal to the current, the maximum speed of the crankshaft, and losses in the linkage system due to friction.
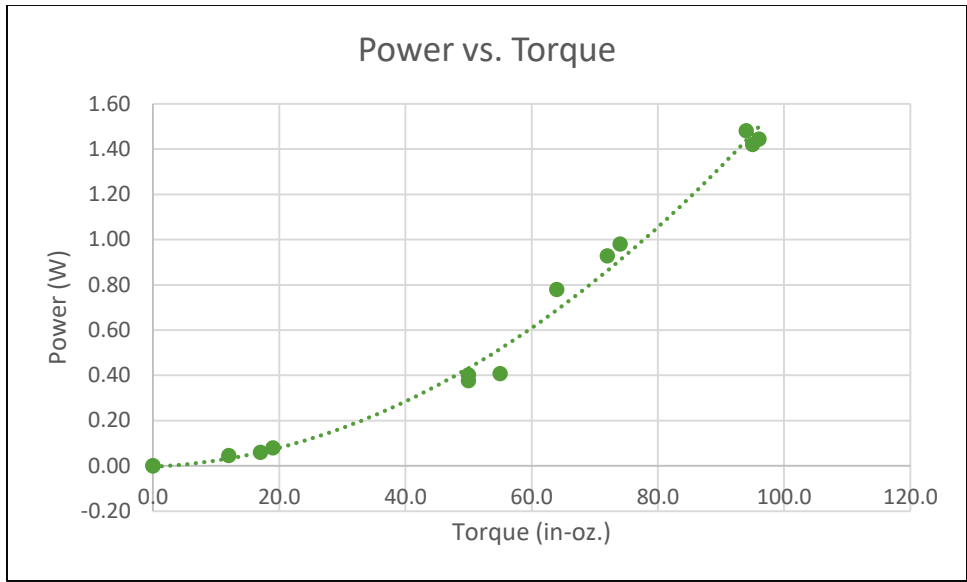
Figure 31: 1/32" 50A Power vs. Torque Graph

Figure 32 displays a curve with an increase in efficiency as the tip speed ratio increases. The tip speed ratio continued to increase at higher speeds while the efficiency of the fin reached a maximum. A parabolic curve is ideal for this graph because there is a peak ratio between the speed of the fin and the speed of the water current.
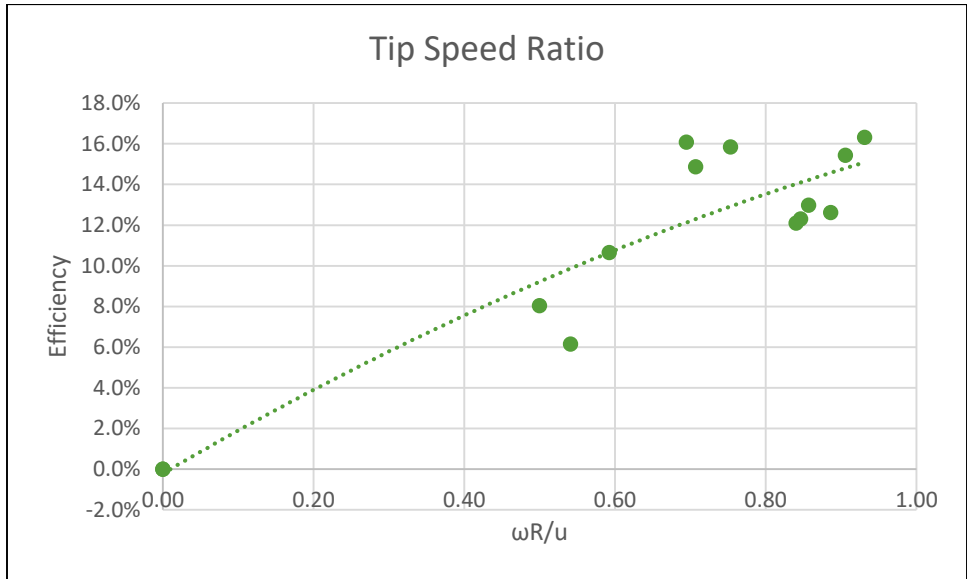

Figure 32: 1/32" 50A Tip Speed Ratio Graph

3/32" 50A Durometer

The second fin tested was constructed out of 3/32" 50A durometer neoprene. This was the only fin tested with this thickness, although the previous fin had the same durometer. Table 3 shows the speed of the water current, the maximum torque of the crankshaft, the RPM of the crankshaft with no load, the actual power, theoretical power, efficiency, and tip speed ratio for each trial. This fin did not move at any water current speeds below 0.75 m/s because there was not enough force on the fin to overcome the static frictional force of the fin. This was a higher threshold speed than the previous fin. A thinner fin worked better in water current speeds lower than 0.75 m/s. The fin produced no data at any speed above 1.25 m/s because the force from the water current was too large and caused the neoprene to fold over and "bunch up" on the masts, preventing the fin from oscillating in the water.

Table 3: 3/32" 50A Data Table

Thickness: 1/32" 40A						
Speed (m/s)	Torque (in-oz)	RPM	Power (W)	P	Efficiency	ωR/u
0.50	0	0	0.0	0.0	0%	0.0
0.75	38	53	0.2	2.5	9%	0.6
0.75	44	56	0.3	2.5	11%	0.6
0.75	44	56	0.3	2.5	11%	0.6
1.00	93	71	0.8	6.0	13%	0.6
1.00	84	73	0.7	6.0	12%	0.6
1.00	77	75	0.7	6.0	11%	0.6
1.25	92	119	1.3	11.7	11%	0.8
1.25	91	121	1.3	11.7	11%	0.8
1.25	97	116	1.3	11.7	11%	0.8
1.5	0	0	0.0	0.0	0%	0.0

The 3/32" 50A durometer fin reached a torque between 32 in-oz. and 63 in-oz., and an RPM between 39 and 116. These measured values produced power ratings between 0.2 Watts and 0.8 Watts, with a maximum efficiency of 8%.

The maximum efficiency measured was 8% at 70 RPM with a 60 in-oz. torque. This efficiency was not as high as the thinner fins. As shown in Figure 33, efficiency and current speed have a parabolic relationship like the previous fin. Since the lower water current speeds could not turn the crankshaft, the beginning part of the curve is absent. The best water flow speed for the 3/32" 50A durometer fin was approximately 1.0 m/s.
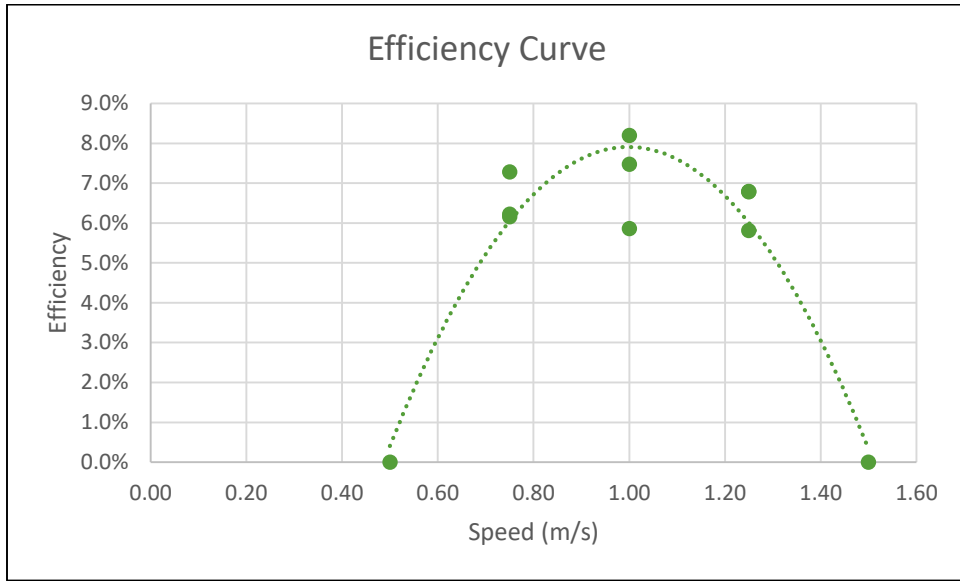
Figure 33: 3/32" 50A Efficiency Curve

The curve in Figure 34 shows that the maximum efficiency for this fin occurred when the torque was 55 in-oz. The data for this fin formed an ideal parabolic curve, as seen in the data for the other fins tested. Once the minimum data point was included, the parabolic curve became more predominant. At 1.5 m/s, the fin did not move, thus creating a maximum point for the efficiency curve.
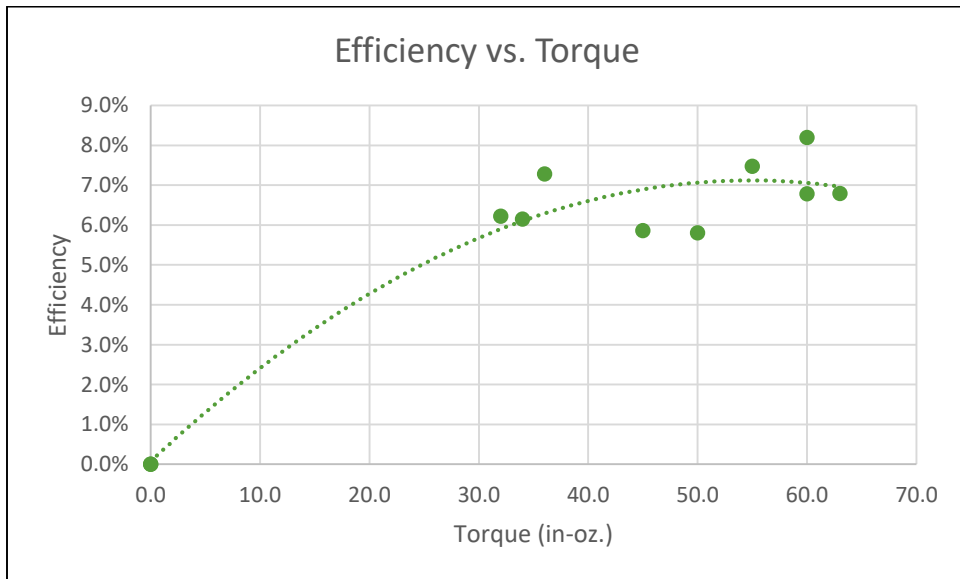

Figure 34: 3/32" 50A Efficiency vs. Torque Graph

As stated previously, the torque and RPM have a direct relationship; therefore, as the RPM increased, the torque of this fin also increased. This fin had a lower torque reading than the previous fin, which resulted in a lower slope. The torque for this fin reached a maximum of 63 in-oz. The RPM for the 3/32" 50A durometer fin was consistently lower than that of the 1/32" 50A durometer fin, and reached a maximum of 108 RPM, as seen in Figure 35.
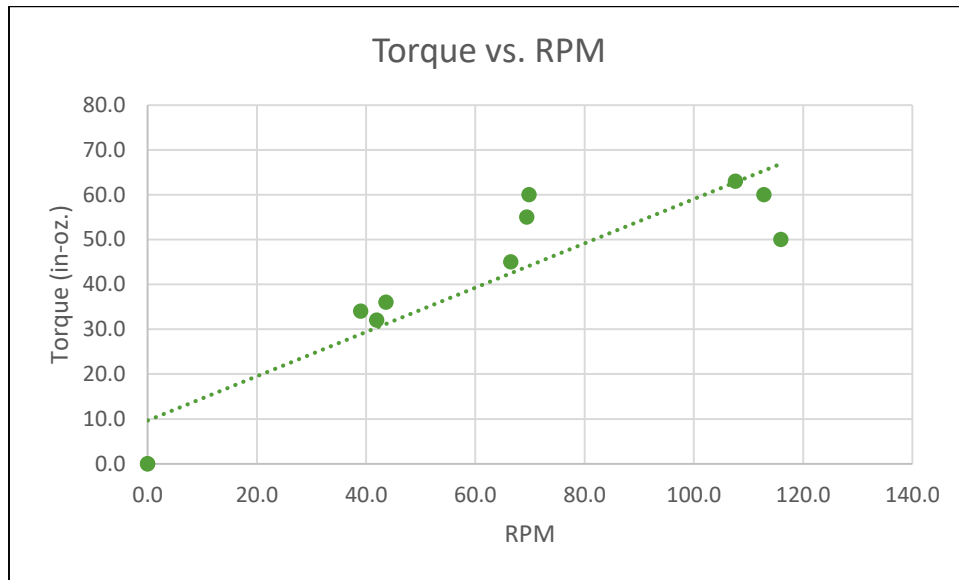

Figure 35: 3/32" 50A Torque vs. RPM Graph

Figure 36 shows the relationship between power and torque for this fin. This fin did not perform as well as the other fins, as the torque values do not go past 70 in-oz. The curve is similar to the shape of the power vs. torque graph for the previous fin because a maximum power was not achievable within the testing constraints.
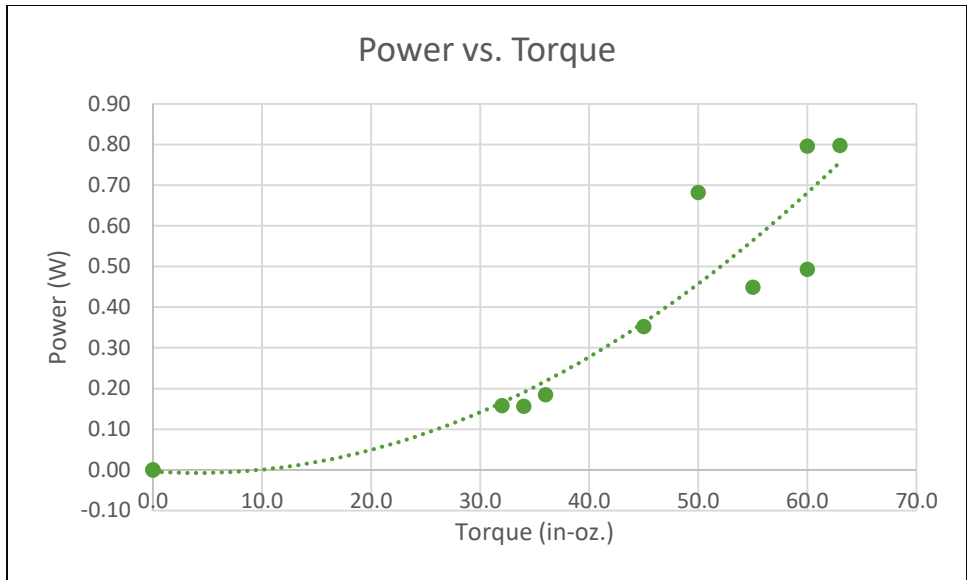
Figure 36: 3/32" 50A Power vs. Torque Graph

The tip speed ratio graph displays a curve that starts with an increase in efficiency as the tip speed ratio increases. The tip speed ratio continued to increase at higher speeds while the efficiency of the fin reached its maximum at a tip speed ratio of 0.6, resulting in the parabolic curve, shown in Figure 37. The parabolic curve is predominant for this fin and is ideal for this graph because the peak ratio between the speed of the fin and the speed of the water current exists.
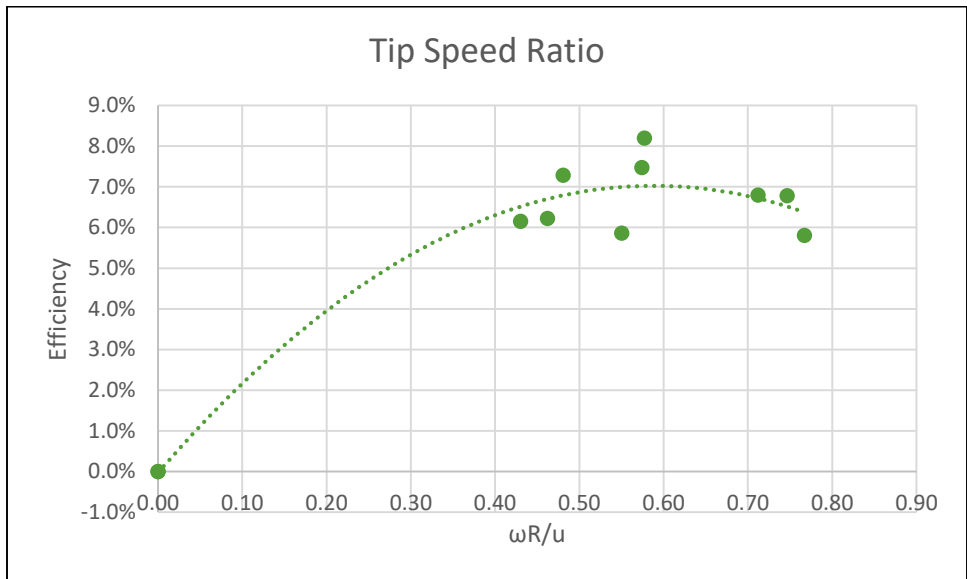

Figure 37: 3/32" 50A Tip Speed Ratio Graph

The next fin tested was made of 1/32" 40A durometer neoprene. This was the second fin tested of this thickness, but this fin had a lower durometer. Table 4 shows the speed of the water current, the maximum torque of the crankshaft, the RPM of the crankshaft with no load, the actual power, theoretical power, efficiency, and tip speed ratio for each trial. It did not move at any water current speeds below 0.75 m/s because there was not enough force on the fin to overcome the static frictional force of the fin, similar to the 3/32" thick fin. This was a higher threshold speed than 1/32" 50A durometer fin, which proved that the durometer of this fin was too low in this case. The fin produced no data at any speed above 1.25 m/s because the force from the water current was too large and the fin folded over.

Table 4: 1/32" 40A Data Table

Thickness: 1/32" 40A						
Speed (m/s)	Torque (in-oz)	RPM	Power (W)	P	Efficiency	ωR/u
0.50	0.0	0.0	0.0	0.0	0%	0.0
0.75	38.0	53.0	0.2	2.5	9%	0.6
0.75	44.0	56.0	0.3	2.5	11%	0.6
0.75	44.0	56.2	0.3	2.5	11%	0.6
1.00	93.0	71.4	0.8	6.0	13%	0.6
1.00	84.0	73.3	0.7	6.0	12%	0.6
1.00	77.0	75.3	0.7	6.0	11%	0.6
1.25	92.0	118.7	1.3	11.7	11%	0.8
1.25	91.0	120.8	1.3	11.7	11%	0.8
1.25	97.0	115.8	1.3	11.7	11%	0.8
1.5	0.0	0.0	0.0	0.0	0%	0.0

The 1/32" 40A durometer fin reached a torque between 38 in-oz. and 97 in-oz., and an RPM between 53 and 121. These measured values produced power ratings between 0.2 Watts and 1.3 Watts, with a maximum efficiency of 13%.

The maximum efficiency measured was 13% at 71 RPM with a 93 in-oz. torque. This efficiency was not as high as the other fin with the same thickness. Figure 38 shows that the efficiency and current speed have a parabolic relationship. Similar to the 3/32" fin, the lower water current speeds could not turn the crankshaft, which caused the beginning part of the parabolic curve to be absent. The RPM and torque of the crankshaft had a direct relationship with the flow speed of the water; however, the torque did not increase in a consistent interval

with higher flow speeds. This is why the efficiency of the fin decreased at the end of the curve.
Based on the parabolic curve in Figure 38, the best water flow speed for the 1/32" 40A
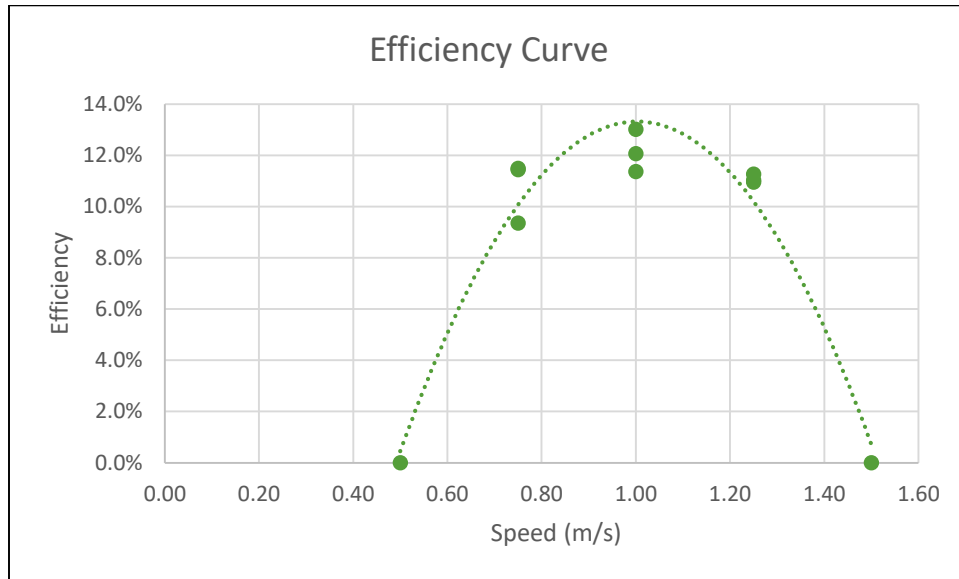durometer fin was approximately 1.0 m/s.

Figure 38: 1/32" 40A Efficiency Curve

Figure 39 shows that the maximum efficiency for this fin occurred when the torque was
75 in-oz. The parabolic curve is less predominant than the one shown for the 1/32" 50A
durometer fin. This was because the torque could not be recorded at 0.5 m/s. Once the peak
efficiency was reached, the torque for this fin increased while the efficiency decreased.
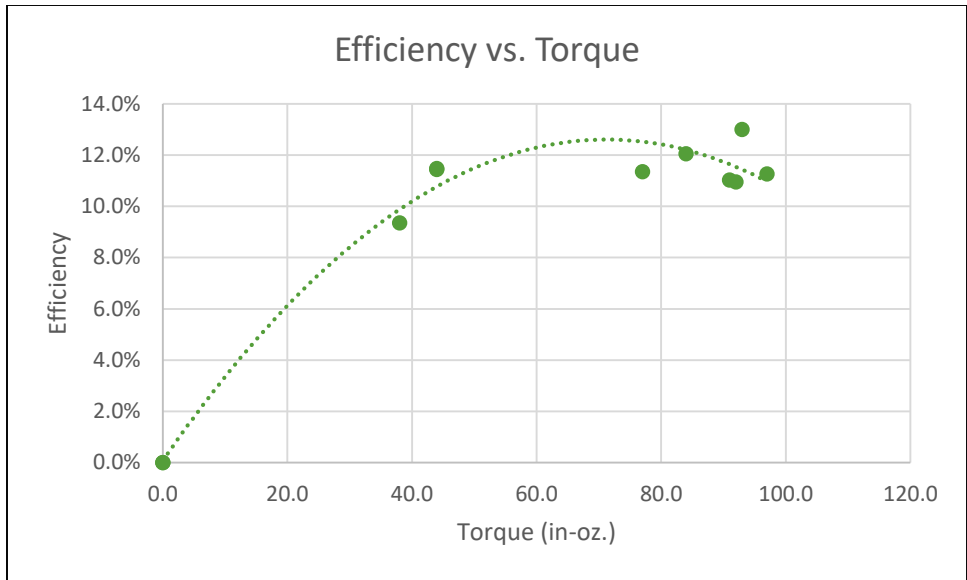
Figure 39: 1/32" 40A Efficiency vs. Torque Graph

Figure 40 further demonstrates that torque and RPM have a direct relationship; as the RPM increased, the torque also increased. At the maximum torque reading of 97 in-oz., the device reached a reading of 116 RPM.
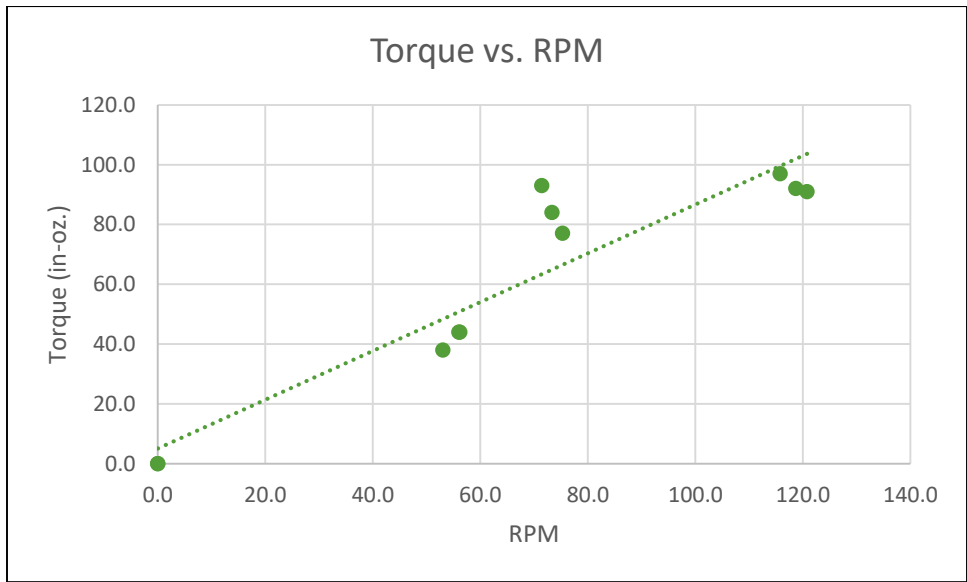

Figure 40: 1/32" 40A Torque vs. RPM Graph

Figure 41 shows the relationship between the power and the torque measured. The torque values did not go past 100 in-oz. due to the range of the torque watch. As the torque reached its maximum potential, the power drastically increased.
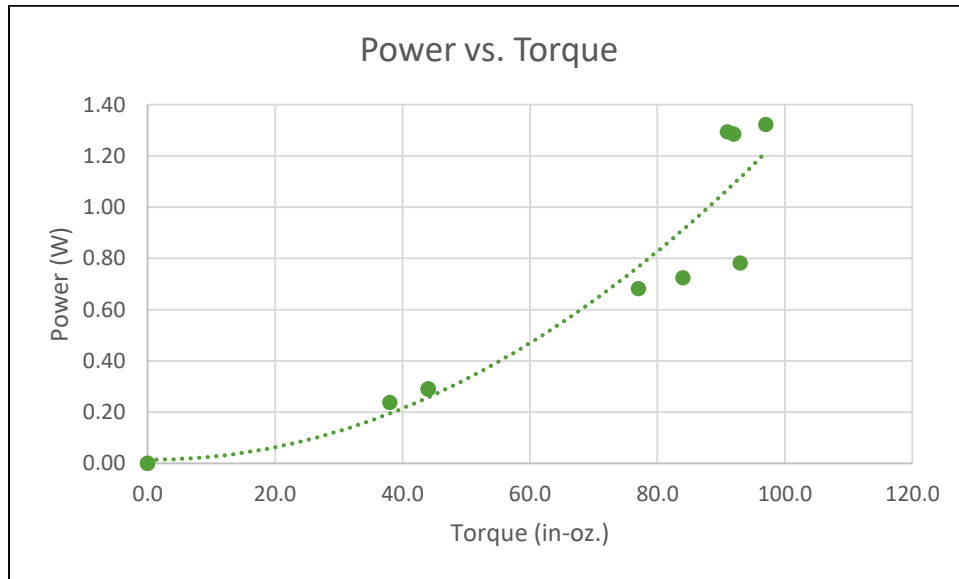

Figure 41: 1/32" 40A Power vs. Torque Graph

The tip speed ratio graph displays a curve that starts with an increase in efficiency as the ratio increases. The tip speed continued to increase at higher water current speeds while the efficiency of the fin reached its maximum at a tip speed ratio of 0.7. This trend resulted in the parabolic curve in Figure 42.
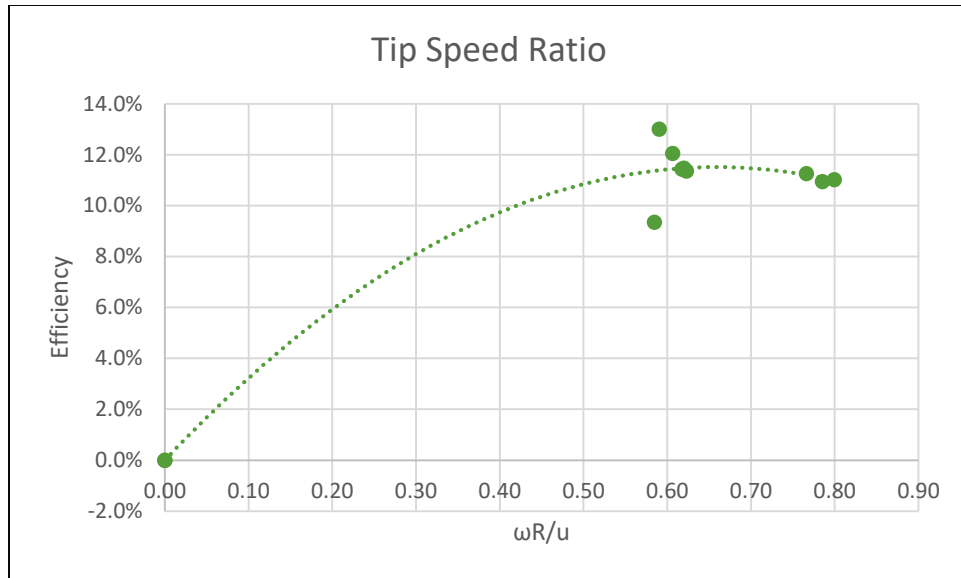
Figure 42: 1/32" 40A Tip Speed Ratio Graph

1/8" 50A Durometer

The ⅛" 50A durometer fin was the thickest fin tested. There was no speed within the range of 0.5 m/s to 2.0 m/s that moved the fin and turned the crankshaft. This thick fin was too rigid and unable to move out of its original shape from the force of the water current moving past it. The mass of the neoprene in this case was too large, so the kinematic force could not overcome the static force acting on the fin. Therefore, the fin was restricted, and the sinusoidal motion was not achievable as the water moved around it, as shown in Figure 43. If the entire device and the fin were larger, there would be more fin surface area in the water and a larger force would act on the fin. The adjustment in size might allow this thick fin to turn the crankshaft and can be further explored by other groups.
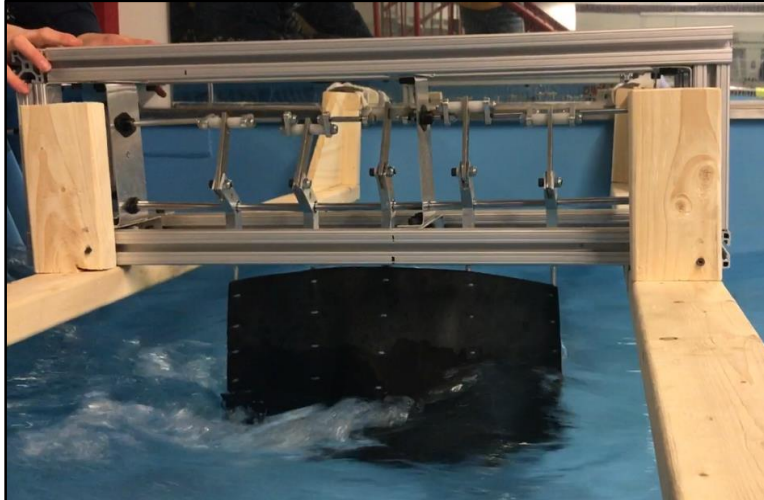
Figure 43: Image of 1/8" 50A Fin in Water

4.3 Generator Verification

The generator verified the results found above from the torque watch and tachometer. This generator, shown in Figure 44, was from Pacific Sky Power, and its original use was for a wind turbine attachment. For testing, the shaft of the generator was attached to the crankshaft. As the crankshaft rotated, it spun the brushed DC motor and produced a voltage and current. The leads of the generator were attached to an electrical circuit and LCD meter that output the power produced. Results of the generator ranged from 0.01 Watts to 1.5 Watts. This generator could be used to charge a battery or power other small devices when attached to the crankshaft. See Appendix A for the data gathered by using the generator.


Figure 44: Pacific Sky Power Wind Turbine Generator Connected to the Crankshaft

4.4 Testing Limitations

Unfortunately, there were limitations to the data produced and discussed above. These limitations caused lower efficiencies to occur for each fin. The testing limitations included:

- The device was not securely mounted to the testing frame and would begin to move and shake at current speeds greater than 1.25 m/s and as a result, data was not able to be gathered past this speed.
- The neoprene fins were only 12" tall and 24" wide. If the fin was larger, there would have been more surface area normal to the water current force acting on it.
- The entire fin was not submerged in the rowing tank because the testing frame was too tall. Each fin was submerged approximately 5" into the water. If more of the fin was submerged, more power would have been generated.
- During the tests, some of the zip ties ripped off as a result of the strong force from the water current. The fin did not move in a perfect sinusoidal motion because there were less contact points between the masts and the neoprene.
- The zip ties attaching the fin to the masts slid down the masts at higher testing speeds. At speeds above 1.25 m/s, the fin would "bunch up" on the masts, as seen in Figure 45.
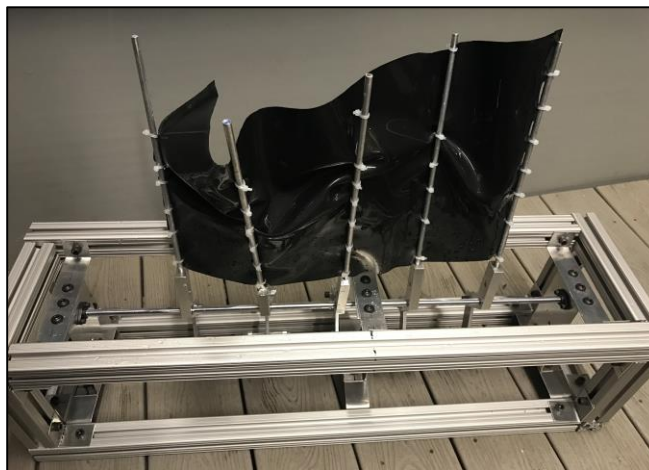
Figure 45: Fin Folded Over

- During one of the tests, a mast became unscrewed from the threaded hole in the linkage. This changed the shape of the fin moving in the current and this data was omitted.

- The torque watches only read up to 100 in-oz.
- While the tachometer was rated to have a high accuracy, it was not always possible to get a clear reading from the device.
- For each fin, there was a maximum speed after which the device would not function. This speed was different for each fin.
- It was not possible to completely control the speed of the water current. The controls for the rowing tank did not directly correspond to flow speed. A table was created based off of testing data for the tank setting and approximate flow speed (based upon a reading taken with a flow meter). Additionally, the current did not scale up in consistent increments, so it was difficult to achieve the same exact setting for every trial. For instance, a setting of 800 on the rowing tank control panel corresponded to a current speed of 1 m/s; however, it was impossible to set the tank to exactly 800 and the setting would range between 790 and 800.
- Turbulent flow from the current also affected the testing results. Turbulent flow occurs when the Reynolds number exceeds 4000 for fluid flow in an open channel. However, the flow of water in the tank is supercritical, because the Froude number is greater than 1. This means that the wake from the movement of the fin will not interfere with the water flowing past it. Table 5 shows the Reynolds and Froude numbers for the water current in the tank for each current speed tested.

Table 5: Reynolds Number for Turbulent Flow

Water speed (m/s)	Re	Fr
0.50	64,000	1.1
0.75	95,000	1.7
1.00	130,000	2.3
1.25	160,000	2.8

Despite the testing limitations, the results obtained during testing were indicative that the device worked properly and confirmed the relationships between testing variables.

5.0 Conclusion

This project focused on designing, manufacturing, testing, and analysis of a hydrokinetic energy harvesting device. Ideally, this could be commercially available to get individual houses off the grid and could help consumers reduce their environmental. The device was comprised of a crankshaft mounted to a neoprene fin via a linkage system. A series of neoprene fins of varying hardness and durability were tested. Fins that were thinner and more durable performed better during testing. The most successful fin was the 1/32" 50A neoprene. The maximum power output of the device was 1.5 Watts, and the maximum efficiency achieved was 16%.

The team decided to design a crankshaft rather than a previously constructed camshaft for many reasons. There are many losses due to friction in a camshaft from the metal ball bearings. In a crankshaft, there are only a few contact points near the brackets that could have minimal friction. These points were reinforced with low friction bearings in the prototype. The crankshaft was secured with lock nuts and Loctite to prevent any components from moving. Ideally, the crankshaft could be welded as one unit.

The four fins that were tested with the crankshaft included: a 1/32" 50A neoprene fin, a 3/32" 50A neoprene fin, a 1/32" 40A neoprene fin, and a ⅛" 50A neoprene fin. Each fin had a maximum efficiency for the flow speed it was tested in. The team concluded that the thinner fins tested in flow speeds between 0.5 and 1.5 m/s flow speeds resulted in higher efficiencies.

Even though the cast silicone fin and the fin mold were ultimately not successful, they provided information and learning opportunities that could be beneficial for future work. If a group continued this project, they could explore more mold materials, mold configurations, and casting materials. These improvements could lead to higher efficiencies and better manufacturing techniques for the device.

In the future, a better testing facility is necessary to control the testing conditions and to more precisely collect data. The rowing tank at WPI is limited because of the depth of the water, the range of water flow speeds, and the time the team was allowed to use the facility. An ideal situation would include using a testing facility off-campus designed specifically for testing hydropower devices. Additionally, the size of the prototype was constrained by the testing facilities available. A larger prototype would be necessary to better understand the full capacity

of the device. Theoretically, if the device was larger in size, there would be a larger power output and a higher efficiency. However, size is also limited by cost and construction time.

The device constructed in this project had advantages over traditional hydropower turbines. The simplistic design of the crankshaft allowed for ease in manufacturing and assembly of each linkage, and the size of the prototype was best suited for slow water currents. This device also has potential for interchangeable fins, which would make maintenance easier than fixing a turbine. Furthermore, the shape of the fin allows fish to swim around it. This creates a symbiotic relationship between marine life and the device.

In comparison to other energy sources commercially available, industrial hydro-turbines today are able to convert up to 90% of the available energy to electricity. This is a much larger efficiency than the most efficient fossil fuel plants, which have up to a 50% efficiency [29]. While these sources are much more efficient than the device created for this project, most home solar panels have a 10-20% efficiency [30]. This efficiency can compare to the 16% efficiency found from the prototype in this project because it has a similar intended application. For the device to be commercially competitive, the cost per kilowatt hour generated would need to be less than $0.15 per kilowatt hour of electricity generated in order to remain competitive with solar panels.

Overall, this project was a success. It added to research done by previous groups to show that it is possible to efficiently generate power from a river current using a fin and a crankshaft. With continued research, development, and experimentation, this hydrokinetic river current power generation device has the potential to be continued by other project teams. However, it currently does not show potential for development commercially, unless the design were to be simplified and the efficiency improved. Additional studies would need to be conducted to determine if the device would be competitive with other alternative energy devices.

Bibliography

[1] "Wave energy devices that harness wave energy," Alternative Energy Tutorials, 2010. [Online]. Available: http://www.alternative-energy-tutorials.com/wave-energy/wave-energy-devices.html. Accessed: Sep. 23, 2016.

[2] R. Carballo and G. Iglesias, "A methodology to determine the power performance of wave energy converters at a particular coastal location," *Energy Conversion and Management*, vol. 61, pp. 8–18, Sep. 2012. [Online]. Available: http://www.sciencedirect.com/science/article/pii/S0196890412001343. Accessed: Sep. 23, 2016.

[3] M. J. Khan, M. T. Iqbal, and J. E. Quaicoe, "River current energy conversion systems: Progress, prospects and challenges," *Renewable and Sustainable Energy Reviews*, vol. 12, no. 8, pp. 2177–2193, 2016. [Online]. Available: http://www.sciencedirect.com/science/article/pii/S136403210700069X. Accessed: Sep. 23, 2016.

[4] E. J. Tarbuck, F. K. Lutgens, and D. Tasa, *Earth: An introduction to physical geology*, 10th ed. United States: Pearson Prentice Hall, 2010.

[5] "Hydrokinetic in-stream Turbines," *SMART HYDRO POWER*. [Online]. Available: http://www.smart-hydro.de/renewable-energy-systems/hydrokinetic-turbines-river-canal/. [Accessed: 19-Mar-2017].

[6] A. M. Hudzik, "Hydrokinetic Oscillators for Energy Harvesting vis Coupling Polyvinylidene Fluoride (PVDF) and Electromagnetics," University of Pittsburgh, Pittsburg, PA 2007. Available: http://d-scholarship.pitt.edu/8661/1/AMHudz_MSThesis.pdf. Accessed: March 18, 2017.

[7] "Hydropower from Vortex-Induced Vibrations," *The Future Of Things*, 26-Oct-2013. [Online]. Available: http://thefutureofthings.com/3889-hydropower-from-vortex-induced-vibrations/. [Accessed: 19-Mar-2017].

[8] J. Widén *et al.*, "Variability assessment and forecasting of renewables: A review for solar, wind, wave and tidal resources," *Renewable and Sustainable Energy Reviews*, vol. 44, pp. 356–375, Apr. 2015.

[9] L. A. Teran *et al.*, "Failure analysis of a run-of-the-river hydroelectric power plant," *Engineering Failure Analysis*, vol. 68, pp. 87–100, Oct. 2016.

[10] R. A. McManamay, N. Samu, S.-C. Kao, M. S. Bevelhimer, and S. C. Hetrick, "A multi-scale spatial approach to address environmental effects of small Hydropower development," *Environmental Management*, vol. 55, no. 1, pp. 217–243, Sep. 2014.

[11] D. Anderson, H. Moggridge, P. Warren, and J. Shucksmith, "The impacts of 'run-of-river' hydropower on the physical and ecological condition of rivers," *Water and Environment Journal*, vol. 29, no. 2, pp. 268–276, Oct. 2014.

[12] L. Hammar *et al.*, "A probabilistic model for Hydrokinetic turbine collision risks: Exploring impacts on fish," *PLOS ONE*, vol. 10, no. 3, p. e0117756, Mar. 2015.

[13] O. Langhamer, K. Haikonen, and J. Sundberg, "Wave power—Sustainable energy or environmentally costly? A review with special emphasis on linear wave energy converters," *Renewable and Sustainable Energy Reviews*, vol. 14, no. 4, pp. 1329–1335, May 2010.

[14] R. Pelc and R. M. Fujita, "Renewable Energy from the Ocean," Marine Policy, Oakland, CA, 2002.

[15] "Marine Corrosion Explained,". [Online]. Available: http://www.marinecorrosionforum.org/explain.htm. Accessed: Sep. 16, 2016.

[16] J. Horton, "How ocean currents work," HowStuffWorks, 2008. [Online]. Available: http://science.howstuffworks.com/environmental/earth/oceanography/ocean-current3.htm. Accessed: Sep. 19, 2016.

[17] C. Fairclough, "Currents, waves, and tides: The ocean in motion," Ocean Portal | Smithsonian, 2016. [Online]. Available: http://ocean.si.edu/ocean-news/currents-waves-and-tides-ocean-motion. Accessed: Sep. 16, 2016.

[18] "Current," in *National Geographic*, National Geographic Society, 2011. [Online]. Available: http://nationalgeographic.org/encyclopedia/current/. Accessed: Sep. 15, 2016.

[19] "What is Biomimicry?," in *Biomimicry Institute*, Biomimicry Institute, 2015. [Online]. Available: https://biomimicry.org/what-is-biomimicry/#.V9__o5grK00. Accessed: Sep. 18, 2016.

[20] K. Davis, D. Reardon, and D. Clegg, "Swimming Fin,", Jun. 16, 2014.

[21] T. Hu, L. Shen, L. Lin, and H. Xu, "Biological inspirations, kinematic modeling, mechanism design and experiments on an undulating robotic fin inspired by Gymnarchus niloticus," Mechanism and Machine, Science Direct, Mar. 2009.

[22] "Knife Fish,". [Online]. Available: http://fishbreeds.net/wp-content/uploads/2012/05/knifefish.jpg. Accessed: Sep. 17, 2016.

[23] S. M. Bailey, A. Y. Chan, N. G. Curtis, and L. A. Richard, "Design of a Novel Concept for Harnessing Tidal Stream Power: A Continuation," Worcester Polytechnic Institute, Worcester, MA, 2016.

[24] I. M. Costanzo, A. H. Kelsey, F. M. Ogren, and D. C. Wians, "Design of a Novel Concept of Harnessing Tidal Stream Power," Worcester Polytechnic Institute, Worcester, MA, 2015.

[25] "Rubber Hardness Chart," in MYKIN INC. [Online]. Available: http://mykin.com/rubber-hardness-chart. Accessed: Feb. 27, 2017.

[26] "Characteristic Properties of Silicone Rubber Compounds," Shin Etsu, 2016. [Online]. Available: https://www.shinetsusilicone-global.com/catalog/pdf/rubber_e.pdf. Accessed: Sep. 17, 2016.

[27] E. Tomko and J. Whyte, "Development of Electricity Generation and Sensor Systems for a Hydropower Propagating Wave Turbine," Worcester Polytechnic Institute, Worcester, MA, 2016.

[28] "Crankshaft," *Crankshaft definition | Engineering Dictionary*. [Online]. Available: http://www.engineering-dictionary.org/Crankshaft. [Accessed: 19-Mar-2017].

[29] A. Davison, "Hydroelectric Power," *Renewable Energy, Hydroelectric Power, benefits and cons of hydro energy*. [Online]. Available: http://www.altenergy.org/renewables/hydroelectric.html. [Accessed: 19-Mar-2017].

[30] "Solar Panel Efficiency and Electricity Generated," *Solar Panel Efficiency - 5 Tips To Improve Their Efficiency*. [Online]. Available: http://www.theecoexperts.co.uk/which-solar-panels-are-most-efficient. [Accessed: 19-Mar-2017].

[31] G. T. says, D. A. R. A. says, A. Says, A. d00d says, W. C. says, D. says, J. T. says, A. W. S. S. says, J. M. says, and J. W. says, "How Much Do Solar Panels Cost," *Energy Informative*. [Online]. Available: http://energyinformative.org/solar-panels-cost/. [Accessed: 20-Mar-2017].
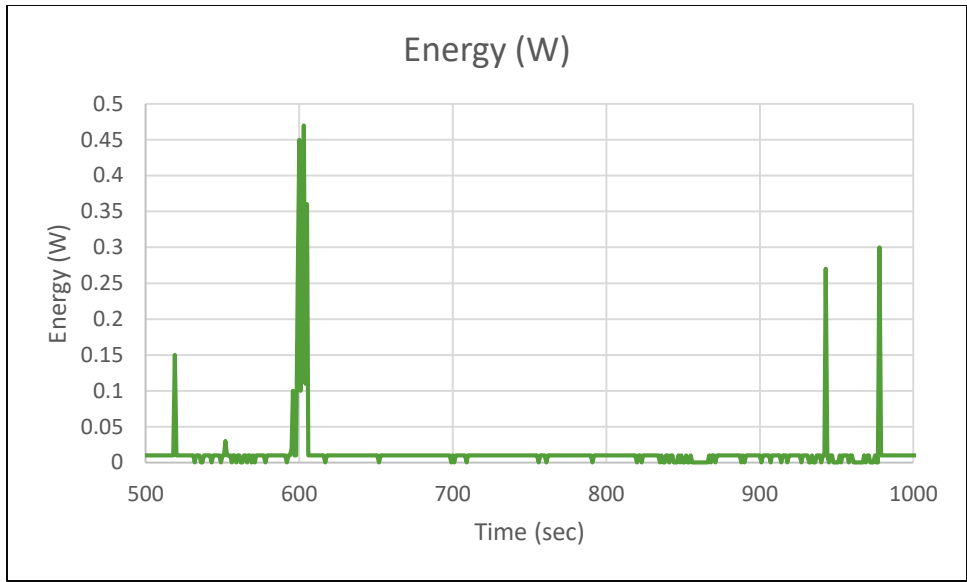
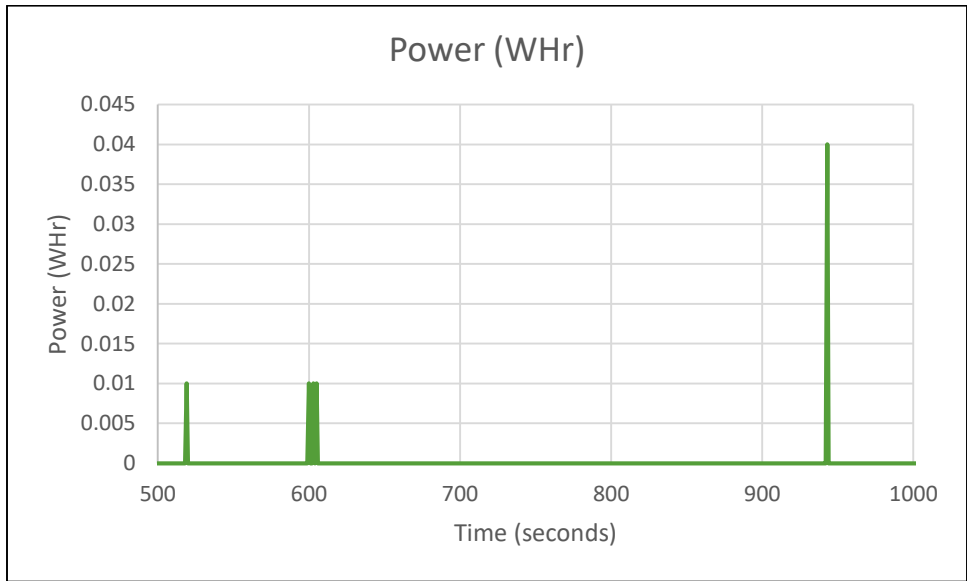# Appendix A: Generator Data
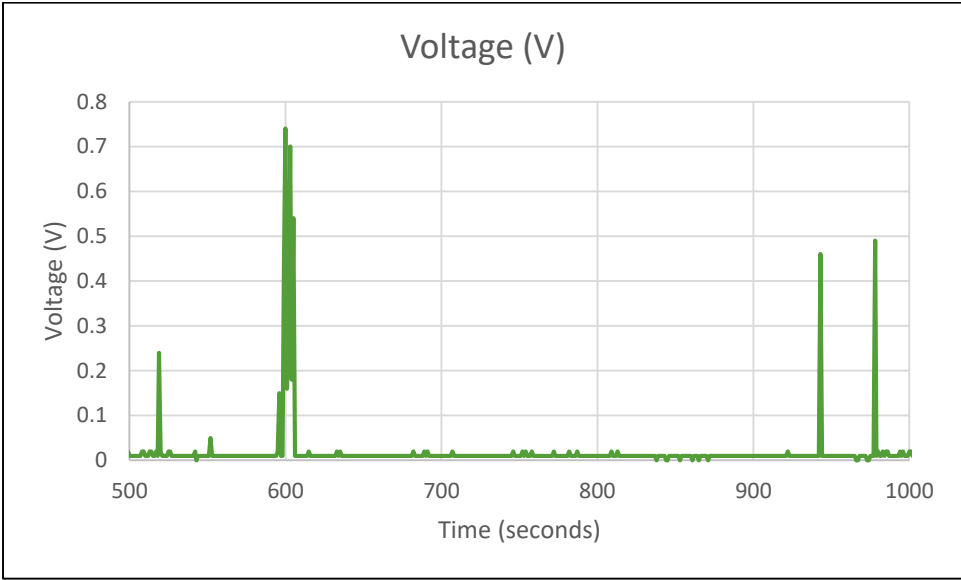
Generator: Voltage Output over Time
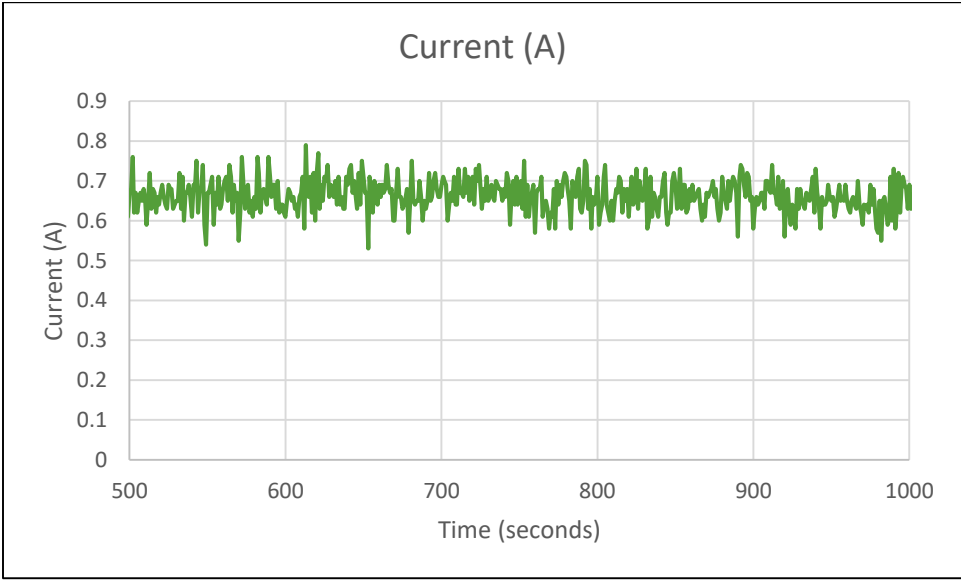
Generator: Current Reading over Time

Generator: Energy Generated over Time

Generator: Power Output over Time